




# A search for Galactic post-asymptotic giant branch stars in *Gaia* DR3<sup>★</sup>

I. González-Santamaría<sup>1,2</sup> , M. Manteiga<sup>2,3</sup> , A. Manchado<sup>4,5,6</sup>, E. Villaver<sup>4,7</sup> , A. Ulla<sup>8,9</sup> , and C. Dafonte<sup>1,2</sup> 

<sup>1</sup> Universidade da Coruña (UDC), Department of Computer Science and Information Technologies, Campus Elviña s/n, 15071 A Coruña, Spain  
e-mail: [iker.gonzalez@udc.es](mailto:iker.gonzalez@udc.es)

<sup>2</sup> CIGUS CITIC, Centre for Information and Communications Technologies Research, Universidade da Coruña, Campus de Elviña s/n, 15071 A Coruña, Spain

<sup>3</sup> Universidade da Coruña (UDC), Department of Nautical Sciences and Marine Engineering, Paseo de Ronda 51, 15011 A Coruña, Spain  
e-mail: [manteiga@udc.es](mailto:manteiga@udc.es)

<sup>4</sup> Instituto de Astrofísica de Canarias, 38200 La Laguna, Tenerife, Spain

<sup>5</sup> Universidad de La Laguna (ULL), Astrophysics Department, 38206 La Laguna, Tenerife, Spain

<sup>6</sup> CSIC, Madrid, Spain

<sup>7</sup> Agencia Espacial Española, 41015 Sevilla, Spain

<sup>8</sup> Universidade de Vigo (UVIGO), Applied Physics Department, Campus Lagoas-Marcosende s/n, 36310 Vigo, Spain

<sup>9</sup> Centro de Investigación Mariña, Universidade de Vigo, GEOMA, Edificio Olimpia Valencia, Campus Lagoas-Marcosende, 36310 Vigo, Spain

Received 6 March 2023 / Accepted 9 June 2024

## ABSTRACT

**Context.** When low- and intermediate-mass stars leave the asymptotic giant branch (AGB) phase, and before they reach the planetary nebula stage, they enter a very brief and rather puzzling stellar evolutionary stage called post-AGB stage. The post-AGB phase lasts very briefly, about a few thousand years at most. The number of objects that are confirmed in this phase therefore is really small, and our understanding of this elusive stellar evolutionary stage is accordingly very limited.

**Aims.** We provide a reliable catalogue of Galactic post-AGB stars together with their physical and evolutionary properties obtained through *Gaia* DR3 astrometry and photometry. As an added product, we provide information for a sample of other types of stellar objects, whose observational properties mimic those of post-AGB stars.

**Methods.** Post-AGB stars are characterised by their infrared excesses and high luminosities. The publication of precise parallaxes in *Gaia* DR3 made it possible to calculate accurate distances and to revise the derivation of luminosities for post-AGB candidates, so that objects outside the expected luminosity range can be discarded. We started by identifying post-AGB stars or possible candidates from the bibliography, and we then searched for their *Gaia* DR3 counterpart sources. Using the available photometry, interstellar extinction, spectroscopically derived temperatures or spectral types and parallax-derived distances from the literature, we fitted their spectral energy distributions and estimated their luminosities and circumstellar extinctions. By a comparison to models, the luminosity values allowed us to determine which objects are likely post-AGB stars from other target types. Their position in the Hertzsprung-Russell diagram allows a direct comparison with updated post-AGB evolutionary tracks and an estimation of their masses and evolutionary ages.

**Results.** We obtained a sample of 69 reliable post-AGB candidates that meet our classification criteria, which provide their coordinates, distances, effective temperature, interstellar and circumstellar extinction, luminosity, mass, and evolutionary age. In addition, we provide similar data for other stellar objects in our initial compilation, such as supergiant stars and young stellar objects. Our identifications and parameters are compared with others found in the recent literature for the subject.

**Conclusions.** We selected the data with the best precision in parallax and distance to obtain more accurate luminosities, which allowed us to confidently classify the objects of the sample in different stellar phases. In turn, this allowed us to provide a small but reliable sample of post-AGB objects. The derived mean evolutionary time and average mass values agree with theoretical expectations and with the mean mass value obtained in a previous work for the subsequent evolutionary stage, the planetary nebula stage.

**Key words.** virtual observatory tools – stars: AGB and post-AGB – stars: distances – stars: fundamental parameters – Hertzsprung-Russell and C-M diagrams

## 1. Introduction

The stellar phase known as post-asymptotic giant branch (post-AGB) stage is a very fast (a few thousand years) and quite unknown phase that takes place at the end of the lifetimes

<sup>★</sup> Tables A.6 and A.7 are available at the CDS via anonymous ftp to [cdsarc.cds.unistra.fr](ftp://cdsarc.cds.unistra.fr) (130.79.128.5) or via <https://cdsarc.cds.unistra.fr/viz-bin/cat/J/A+A/688/A209>

of low- and intermediate-mass stars, after the AGB phase and before the planetary nebula stage, in which the star ionises the previously ejected envelope. The beginning of the post-AGB phase is not exactly determined, and its onset depends on the stellar mass and metal content. Furthermore, the departure from the AGB phase is defined somewhat arbitrarily in the stellar evolution models. For Vassiliadis & Wood (1993) the AGB mass loss terminates when the envelope mass is reduced to a value at

which the stellar effective temperature increases beyond a reference value by an amount of  $\Delta \log(T_{\text{eff}}) = 0.3$ . Other authors have different criteria. Miller Bertolami (2016) set the onset at the point in time when as a result of stellar winds, the H-rich envelope mass drops below 1% of the stellar mass.

During the post-AGB phase, the star evolves at an almost constant luminosity towards hotter effective temperatures, while its envelope expands into the interstellar medium. Due to the high stellar temperature, this envelope composed of gas and dust begins to be ionised (see e.g. Villaver et al. 2002). At this moment, the star enters the protoplanetary nebula phase. As in González-Santamaría et al. (2021), we can assume a minimum stellar temperature of 13 000 K for a transition stage from a preplanetary nebula (Weidmann et al. 2020) to about 24 000 K for a complete ionisation of the nebula (Kwok 2000).

Several studies have recently been carried out to identify post-AGB stars with the aim to better characterise this brief stellar phase. Garcia-Lario et al. (1997) identified 110 possible post-AGBs based on their IRAS<sup>1</sup> infrared colours, most of which lack an optical counterparts. At the beginning of this century, Suárez et al. (2006) provided optical counterparts for more than 100 post-AGB candidates that were previously proposed as such based on their IRAS fluxes. Almost in parallel, a more extensive catalogue of post-AGB candidates was presented by Szczerba et al. (2007), which was later extended in Szczerba et al. (2012). This is known as the Torun catalogue of post-AGB stars and is the largest catalogue to date. It contains 296 sources classified as either likely or possible post-AGBs. The sample of post-AGB stars has been expanded to the Large Magellanic Cloud (LMC) by Kamath et al. (2015). They also included post-red giant branch (RGB) stars. These stars are thought to be produced from binary interactions in the RGB phase, and their observational properties mimic those of post-AGB stars, although they are not expected to reach luminosities as high as those of post-AGB stars (Kamath et al. 2015). In a previous article (González-Santamaría et al. 2021), we found that a fraction close to 50% of the central stars of PNe are red and might therefore be unresolved binary systems. Finding the relative number of stars of one type and of single or binary type at these evolutionary stages can give us clues about the fraction of binary stars that has evolved companions.

Kamath et al. (2022) recently studied the evolutionary state of 31 Galactic post-AGB candidates with chemical abundance information. By using *Gaia* EDR3 distances and known photometry, they built the spectral energy distribution (SED) for these objects, and by fitting them to models, they estimated their luminosities and temperatures. It is important to note that 20 of the objects they analysed have quite poor astrometry in *Gaia* DR3.

Parthasarathy et al. (2020) analysed the properties of 8 post-AGB candidates based on *Gaia* DR2 astrometric and photometric data. Also using *Gaia*, in this case, DR3, Oudmaijer et al. (2022) investigated their nature as possible post-AGB of 249 objects. It is noteworthy that most of the objects they selected have large uncertainties in their parallaxes, which leads to very unreliable distance values. They considered good parallaxes to have a relative error ( $1\sigma$ ) between 10% and 100%. Additionally, we detected some inconsistencies in their study on which we comment in Sect. 3.

Finally, in a recent work, Aoki et al. (2022) studied the evolutionary state of 20 post-AGB candidates by using *Gaia* DR2 and EDR3.

We aim to identify and analyse the properties of bona fide post-AGB stars in more detail by selecting objects with accurate astrometric measurements in *Gaia* DR3, which allows us to

precisely locate them in the Hertzsprung-Russell (HR) diagram. This consequently leads to a quite reliable classification of these stars as post-AGB objects. If we were to select objects from Galactic post-AGB stars candidates with good astrometry in *Gaia* DR3, we would exclude in a first approximation most astrometric binaries. The general rule is that the threshold of the *Gaia* astrometric quality parameter called renormalised unit weight error (RUWE)  $\leq 1.4$  is used to indicate single well-behaved solutions (Lindgren et al. 2018, 2021). The inconsistency of source observations with the *Gaia* astrometric five-parameter model could be caused by binarity (Lindgren et al. 2018) or other factors that cause the photocentre of the source to wobble during the *Gaia* observation window. In summary, a restrictive criterion in the astrometric quality helps us to select objects that are more likely to be individual sources, and on the other hand, it helps us to estimate their luminosity and evolutionary stage better. The incidence of binaries in our resulting sample is addressed by studying the SED morphology, and we also consider this in the context of the literature.

We started by collecting a sample of post-AGB candidates that was as complete as possible from the currently available catalogues (Sect. 2), and we implemented restrictive filtering over the astrometric quality of the objects so that we only kept those with the most accurate distance values. We gathered a general sample of 964 post-AGB candidates from the literature, out of which we filtered a subset of 178 objects with accurate astrometric measurements in *Gaia* DR3. A good distance determination is not enough to obtain a reliable adjustment of the SED; additional information about the temperature and/or extinction in the direction of the source is required for a consistently derived luminosity of the object. To better constrain the value of the total extinction, interstellar and circumstellar, in the direction of the source, we opted to limit our work to objects with available interstellar extinction measurements in the literature. Of the previous sample of 178 objects, we kept 146 Galactic post-AGB candidate stars with literature values of their interstellar extinction. In this last sample, the information available in the Simbad database as well as images of every sky field in the Aladin Sky Atlas (Bonnarel et al. 2000) were analysed. We finally discarded 28 sources from the further analysis because they were either already classified as PNe (5 objects), had higher effective temperatures in the literature than 24 000 K (11 objects), or because the identification of the optical counterpart was dubious (12 objects). Our final working set was 118 objects. We found that the temperatures for about 67% of them were derived from spectral analysis, and some of these from a high-resolution spectral analysis. The average temperatures for the remainder corresponding to their spectral types were used. Sect. 3.2 describes the problems associated with the different quality of the temperature determinations we used in detail.

Photometry in a wide spectral region compiled by the Spanish Virtual Observatory SED Analyser (VOSA<sup>2</sup>) allowed us to build the SED for each object. The knowledge of distances and temperatures allowed us to obtain luminosities and to estimate the total extinction from the SED fitting (Sect. 3.3). We used the current knowledge of interstellar extinction in the direction of every object to verify the consistency of the total extinction we obtained in the fits.

Based on evolutionary tracks, we used the distribution of objects in an HR diagram to confirm 69 objects out of 118 candidates as post-AGB stars. Some other objects could be classified as horizontal branch stars (3 objects), luminous supergiants (3 objects), young stellar objects (YSOs; 14 candidates), and the

<sup>1</sup> InfraRed Astronomical Satellite.

<sup>2</sup> <http://svo2.cab.inta-csic.es/theory/vosa/>

remaining objects are unconfirmed post-AGB candidates. The details are given in Sect. 3.5. In Sect. 3.6, this classification is compared with the classifications presented in other recent papers about the subject. In Sect. 4, we focus on analysing the evolutionary properties of the set of 69 objects that we identify as belonging to the post-AGB stage. In Sect. 5, we comment on some interesting objects, and in Sect. 6, we summarise our conclusions.

## 2. Sample selection: Method

The first step in this research was to collect all the objects from the literature that were catalogued as confirmed or possible post-AGB stars. For this purpose, we used the online<sup>3</sup> Torun catalogue of Galactic post-AGB stars (Szczerba et al. 2012), the Simbad astronomical database, and the spectroscopic atlas of post-AGB and planetary nebulae by Suárez et al. (2006; from now, the on Suarez et al. catalogue).

We gathered all objects that were catalogued as likely (209) or possible (87) in the Torun catalogue, as post-AGB (331) or post-AGB candidate (507) in the Simbad database, and as post-AGB (102) in the Suarez et al. catalogue. To combine the three catalogues, we first matched the Torun objects with those in Simbad using a cross-match radius of one arcsecond. As a result, we obtained a set of 929 objects. Subsequently, we matched them with Suarez et al. catalogue (by the same method and using coordinates from Torun when possible), obtaining a final sample of 964 objects.

The next step was to cross-match our list of objects with the *Gaia* DR3 archive to obtain their parallaxes and distances. We again used a search radius of 1 arcsec from the literature coordinates. In some cases, the coordinates from Simbad or from the Suárez et al. catalogues differ slightly from the coordinates from the Torun catalogue. This can lead to discrepancies in the identification of the *Gaia* DR3 source. We decided to prioritise the Torun coordinates because they come from a revised compilation of post-AGB stars. As a result, we were able to identify 843 objects as *Gaia* DR3 sources. This is about 87% of the whole sample. Finally, we discarded objects with unknown distances in Bailer-Jones et al. (2021), which left 765 objects.

In *Gaia* DR3, the parallaxes ( $\pi$ ) show a bias or zero point ( $z_0$ ) that should be considered and subtracted from the measured value to obtain the actual parallax ( $\pi_0$ ). According to Lindegren et al. (2021), this zero point has a mean value of  $-17 \mu\text{as}$ , although its value varies depending on the celestial position, colour, and magnitude of the star. The *Gaia* web provides a Python code for estimating this zero point<sup>4</sup>. After obtaining the zero points, we corrected the parallaxes with the following simple expression:

$$\pi_0 = \pi - z_0.$$

The uncertainties in the *Gaia* parallaxes include the value given in the *Gaia* DR3 archive, the internal uncertainty, and a systematic uncertainty that depends on the source brightness. We followed the prescriptions given in Fabricius et al. (2021) to estimate the total parallax uncertainties of our objects.

From the inverse of the parallaxes, it is possible to estimate the stellar distances, but this simple approach is only valid for objects with relative uncertainties as low as 10%. In general, this is not the case for our data, and we therefore used the distances calculated by a Bayesian approach for Milky Way stars by

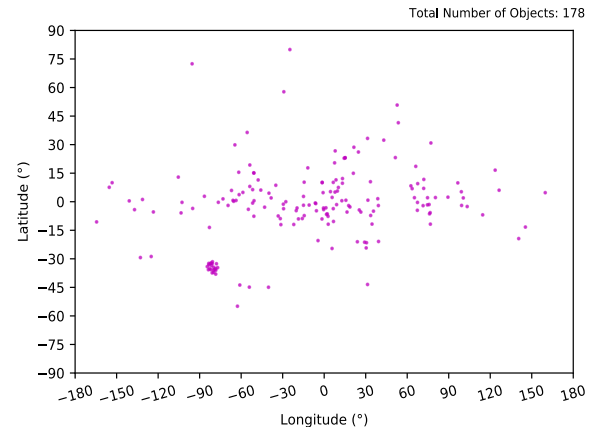


**Fig. 1.** Galactic distribution of the 178 post-AGB candidates from the selected sample.

Bailer-Jones et al. (2021), which consists of assuming an a priori probability volume density of stars in the Galaxy that decreases exponentially on an appropriate distance scale. This method not only provides an estimated distance for a source, but also gives low and high error distance bounds.

To infer useful stellar properties that depend on distance, such as luminosity, it is important to have precise distances to these objects. We therefore decided to apply filtering to our sample according to the distance uncertainties and the astrometric quality. Astrometric quality indices such as the unit weight error (UWE; see the official *Gaia* website) and RUWE beyond certain boundaries prevent *Gaia* users from errors in the astrometric solution that can be due to binarity or to irregularities in the fitted source. We decided to use the same filtering criteria as we used in one of our previous works, where we conducted a similar study, but on the Galactic sample of central stars in planetary nebulae (González-Santamaría et al. 2021). This filtering consisted of the following constraints: The relative error in parallax and distance (for the lower and upper bounds) below 30% and the astrometric quality parameters UWE and RUWE below certain threshold values that are recommended in the *Gaia* documentation ( $UWE < 1.96$  or  $RUWE < 1.4$ ). After applying these constraints, the set contained 178 objects that we consider to have good astrometric measurements in *Gaia* DR3.

The Galactic distribution of these stars shows a small cluster of 21 objects in a region of mid-south latitudes (see Fig. 1) at longitudes coincident with those of the direction of the LMC (Large Magellanic Cloud). Furthermore, we verified that all of these objects were included in the van Aarle et al. (2011) catalogue of LMC post-AGB stars, and 10 of them are also included in Kamath et al. (2015). We therefore decided to exclude these stars from our present study and focused on the remaining 157 Galactic post-AGB candidates.

In Table A.1, we provide general data of the objects in this latter sample: a running number, the name, the *Gaia* DR3 ID, the J2000 coordinates, the *G* magnitude, the interstellar extinction in the *V* band, the spectral type, the reference for an identification as post-AGB (the Torun, Simbad, and Suárez et al. catalogues), and a flag providing information about binarity, variability, and the reason for excluding the source from the further analysis, as described in the previous section, together with a reference.

The distance distribution of all these post-AGB candidates is shown in Fig. 2. We did not attempt to analyse the completeness of the sample since it presents several observational biases,

<sup>3</sup> <https://fox.ncac.torun.pl/camkweb/postagb2.php>

<sup>4</sup> [https://gitlab.com/icc-ub/public/gaiadr3\\_zeropoint](https://gitlab.com/icc-ub/public/gaiadr3_zeropoint)

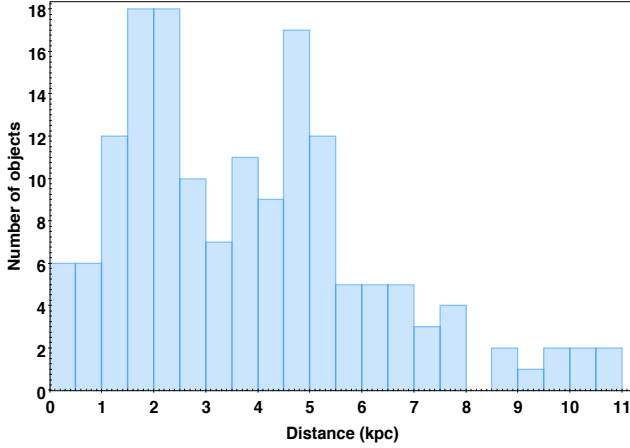


**Fig. 2.** Distance to the 157 Galactic post-AGB candidates with good-quality astrometry.

including the impossibility of detecting the optical counterpart of some of the infrared sources with data in the IRAS catalogue.

Individual distance values in pc, except for discarded objects, are listed in the second column of Tables A.2–A.5.

### 3. Identification of Galactic post-asymptotic giant branch stars

The luminosity of a star is a very useful property for distinguishing between post-AGB stars and other stellar objects with similar colours that are located beyond the main sequence (MS) of the HR diagram, as is the case for YSOs. To narrow the luminosity range that corresponds to post-AGB stars, we resorted to different evolutionary models for hydrogen-burning post-AGB stars: The classical models by Vassiliadis & Wood (1993; for masses between 1 and 5  $M_{\odot}$ ) and by Bloeker (1995; for masses between 1 and 7  $M_{\odot}$ ), and more recently, the model by Miller Bertolami (2016), which includes different metallicities (for masses between 0.8 and 4  $M_{\odot}$ ). Although the range of masses of the progenitor stars is different in each of the models, it should be noted that the evolution of stars with masses greater than 4  $M_{\odot}$  is very fast. Rather poor statistics is therefore expected for objects of these and higher masses. Their expected number is probably also very small given the initial mass function. The models (see Fig. 3) agree reasonably well on a luminosity range of  $3.4 \leq \log(\frac{L}{L_{\odot}}) \leq 4.5$ .

This luminosity range for post-AGB stars meets the criteria used by Kamath et al. (2015), who considered that the luminosity range for post-AGB stars is between 2500  $L_{\odot}$  and 35 000  $L_{\odot}$ . According to these authors, objects above this upper limit may be supergiants or hypergiants, high-mass stars that quickly initiate helium-core fusion after they have exhausted their hydrogen and that continue to fuse heavier elements after helium exhaustion until they develop an iron core, at which point, the core collapses to produce a Type II supernova. In contrast, objects below the lower limit may be post-RGB stars, YSOs, or they may be other evolved stars such as horizontal branch (HB) stars.

The main problem in classifying high-luminosity stars as either post-AGB evolved objects or high-luminosity massive objects is that the two types of objects share many observational features: the optical spectra are similar, they have unstable and extended atmospheres, their gas-dust envelopes expand, they have a high IR excesses, and their IRAS colours are similar

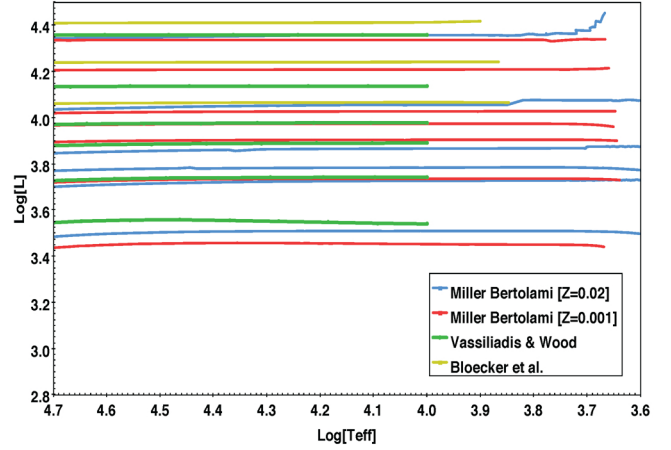


**Fig. 3.** Region in the HR diagram covered by different evolutionary tracks of post-AGB evolution.

(García-Lario et al. 1997). This matter is dealt with in detail by Klochkova & Chentsov (2018), who argued the need to determine and compare various parameters: the position in the Galaxy, the luminosity, the wind parameters, the SED, and the chemical composition to allow for an accurate classification. For this reason, the few objects that we found up to the limit  $\log(\frac{L}{L_{\odot}}) = 4.5$  are discussed individually (see Sect. 5).

Objects below the minimum luminosity indicated by post-AGB evolution models present a different problem. These objects have  $2 < \log(\frac{L}{L_{\odot}}) < 3.4$ . As we mentioned before, in Kamath et al. (2015), the post-AGB candidates in the Magellanic Clouds located in this range were tentatively identified as post-RGB stars. According to these authors, these stars are most likely the result of binary interaction in which their evolution towards the AGB is interrupted, but only in some cases was their binary nature confirmed, and some of them might equally be the result of a merging process. It is beyond the scope of this paper to analyse these objects, and for this reason, we refer to them as unconfirmed post-AGB candidates.

Thus, to classify our objects as post-AGB stars or as another type of stellar objects, it is necessary to calculate accurate luminosities and also to have reliable estimates of their temperatures.

#### 3.1. Interstellar reddening

To explore the best possible determination of the interstellar extinction values for our objects, we used *Gaia* DR3 coordinates and distances and searched the bibliography for the corresponding extinction values. After analysing and comparing data from different catalogues and dust maps, we decided to use the extinction values from Stassun (2019). We obtained  $E(B - V)$  values from this catalogue by performing a cross-match between our objects sample and the TESS<sup>5</sup> Input Catalog v8.0 (Stassun 2019) using the Topcat tool (Taylor 2005). The Stassun catalogue contains extinctions from dust maps for 146 objects of our sample. We always used distance-dependent extinction values when they were available. Extinction errors are provided for 116 objects, and the magnitudes of about 80% of them are below  $\Delta A_V = 0.15$ . The interstellar extinction values are listed in Table A.1.

<sup>5</sup> Transiting Exoplanet Survey Satellite.

### 3.2. Effective temperatures

We searched the Simbad database for temperature values and references for each object in our sample of 146 candidates. As a result, we discarded 28 objects that were too hot or for which the identification of the central source in the literature was uncertain. In consequence, we ended up with a sample of 118 objects, that we considered our final sample. The details are included in Table A.1. We found very different temperature values. Approximately 67% of objects have precise temperature determinations that come from spectral analysis. This is the case of 11 objects in common with the work of Kamath et al. (2022), or those in common with Corporaal et al. (2023) or Mello et al. (2012; see references in Tables A.2–A.5).

For several cases, the  $T_{\text{eff}}$  come from spectral types derived from medium-resolution spectra, as in the Suárez et al. (2006) catalogue. For other cases, only Simbad spectral types are available, some of which cover a quite wide range of subtypes or even types. We also note that for some objects, the spectral classifications in the MK system, which are generally old, are quite discrepant with the spectroscopic temperatures obtained in more recent publications. For instance, the star BD+48 1220 is assigned spectral type A4Ia (8550 K) in Simbad based on Hardorp et al. (1965), while Ting et al. (2019) reported a value of 6389 K from an APOGEE spectra analysis. This leads us to deduce that at least for some cases, the effective temperatures obtained from spectral types may be inaccurate.

Following the precision of the literature values, the temperatures from spectral analysis were prioritised over temperatures obtained by spectral classification in MK types, which in turn were prioritised over average temperatures obtained directly from the spectral type in the Simbad database. Tables A.2–A.5 list the effective temperature we adopted for each object together with a reference and a flag indicating its origin.

### 3.3. Luminosity and total extinction from fitting the spectral energy distribution

To estimate the luminosity of a star, its bolometric flux or magnitude, distance, and interstellar extinction values are needed. A simple approach consists of obtaining the stellar photospheric magnitude  $V$  and then applying the bolometric correction to derive the bolometric magnitude. Alternatively, stellar photometry in several bands can be used to build the SED, and then, by fitting it to a certain model, the stellar temperature and luminosity can be predicted. This simple approach is not possible in most cases because of the dust in the interstellar medium, which reddens the spectral distribution and converts the determination of parameters by fitting with a model into a degenerate problem between temperature and extinction.

We assumed as valid the temperature values obtained from the literature with the method explained in the previous section. We then used a procedure that allowed us to obtain the luminosity by fitting the SED, introducing the total extinction necessary to obtain the already known temperature value within a range of 250 degrees, which can be considered an acceptable value for the errors of the temperatures assigned from the literature to each object.

The VOSA software is the Spanish Virtual Observatory tool that was designed, among other uses, to estimate effective temperature ( $T_{\text{eff}}$ ), gravity, and luminosity based on stellar photometry. The user provides the coordinates of the source, the source distance, and its uncertainties, and the system searches

for observed flux (and their errors) by querying several photometric catalogues accessible through VO services to achieve as wide a wavelength coverage of the data to be analysed as possible. We were then able to choose among different stellar models to perform the fitting. We chose Kurucz models (Castelli & Kurucz 2003) because they are well fitted for our range of temperatures and the evolutionary stage of post-AGB stars. The VOSA software then performed the absolute flux calibration of the observational data, using the information for the available filters (zero points, transmission curves, etc.).

Next, the software determines the synthetic photometry for the models with physical parameters in the range selected by the user (in our case,  $\log[g]$  values between 0 and 5 and a metallicity between  $-4$  and 0.5). Dust extinction is also an input to the system. It is provided without uncertainty together with the selection of an appropriate extinction law. The VOSA tool makes use of the extinction law by Fitzpatrick (1999) that was improved by Indebetouw et al. (2005) in the infrared. Next, the best-fitting model is provided by VOSA, together with the derivation of the corresponding stellar parameters:  $T_{\text{eff}}$  and luminosity (and a value for  $\log[g]$ , the metallicity, and the overabundances of  $\alpha$ -elements with respect to iron).

In the problem that interests us, we carried out an iterative procedure that consisted of providing an input test value of the extinction (starting with a value close to the interstellar extinction value from 3D maps) and determining the temperature value that was obtained in the SED fitting. We then modified the extinction value in steps of 0.05 magnitude until a temperature value closer to the literature value within the uncertainty of 250 K mentioned before was obtained. The total extinction values obtained from the SED fit can be compared with those from the extinction maps to derive the contribution of the circumstellar component.

Post-AGB candidates in the Torun catalogue were identified as objects with an infrared excess due to the presence of a dust envelope or a disc. This means that this infrared excess should be accounted for when fitting the SEDs. In VOSA, the excess is detected by iteratively calculating (adding a new data point from the SED at a time) in the mid-infrared (wavelengths redder than  $2.5 \mu\text{m}$ ) the  $\alpha$  parameter as defined in Lada et al. (2006). The theoretical spectral models used by VOSA are based on stellar atmospheres. As a result, the tool only considers the data points of the SED to calculate the fit errors that correspond to bluer wavelengths than the wavelength in which the excess has been flagged.

The VOSA service can be used to build SEDs by querying a large variety of photometric surveys available on the platform. In general, we found fluxes for our objects from several catalogues that covered the ultraviolet, visible, and near-infrared wavelengths. The most common flux sources we used are 2MASS<sup>6</sup>, DENIS<sup>7</sup>, IRAS, spaci, WISE<sup>8</sup>, Tycho, Paunzen, UB<sup>9</sup>, *Gaia* DR3, *Gaia* XPy, Pan-Starrs, and GALEX. The flux ranges are shown in the figures in Tables A.6 and A.7 (available at the CDS)<sup>10</sup>, and the individual fluxes for each object are listed in Table A.6 and Table A.7 (only available at the CDS). The SEDs we provide were analysed to check for bad data points and were then fitted to Kurucz models (Castelli & Kurucz 2003). We found these models very well suited for our sample because they cover a wide temperature range, from 3500 K to 50 000 K.

<sup>6</sup> Two Micron All-Sky Survey.

<sup>7</sup> Deep Near Infrared Survey.

<sup>8</sup> Wide-field Infrared Survey Explorer.

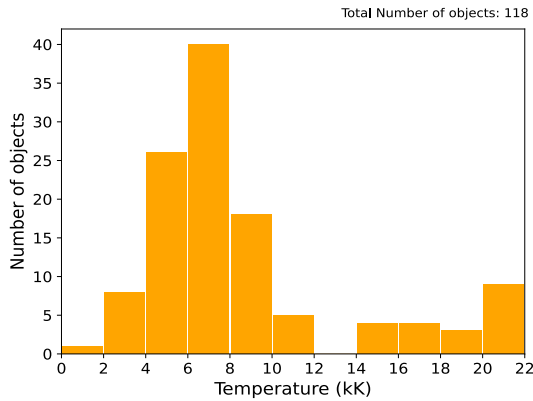
<sup>9</sup> Ultraviolet-Blue-Visible.

<sup>10</sup> <https://zenodo.org/uploads/11569760>

**Table 1.** Temperature, total extinction and luminosity values for the 11 objects in common with Kamath et al. (2022).

Object	$A(V)^{(1)}$ (mag)	$A(V)^{(2)}$ (mag)	$T_{\text{eff}}^{(1)}$ (K)	$T_{\text{eff}}^{(2)}$ (K)	$\text{Log}[L]^{(1)}$	$\text{Log}[L]^{(2)}$
HD 56126	2.0	1.33 <sup>(*)</sup>	7250 ± 125	7485 ± 250	3.94 <sup>+0.04</sup> <sub>-0.05</sub>	3.74 <sup>+0.05</sup> <sub>-0.04</sub>
<b>HD 107369</b>	0.3	0.22	7500 ± 125	7533 ± 250	2.99 <sup>+0.06</sup> <sub>-0.06</sub>	2.96 <sup>+0.04</sup> <sub>-0.05</sub>
HD 133656	1.0	0.90	8250 ± 125	8238 ± 250	3.74 <sup>+0.04</sup> <sub>-0.04</sub>	3.72 <sup>+0.04</sup> <sub>-0.03</sub>
HD 148743	0.6	0.34	6750 ± 125	6728 ± 250	4.51 <sup>+0.07</sup> <sub>-0.08</sub>	4.41 <sup>+0.07</sup> <sub>-0.06</sub>
HD 161796	0.75	0.40	6000 ± 125	6139 ± 250	3.88 <sup>+0.04</sup> <sub>-0.05</sub>	3.76 <sup>+0.04</sup> <sub>-0.04</sub>
HD 187885	1.8	1.74	8000 ± 125	8239 ± 250	3.89 <sup>+0.14</sup> <sub>-0.21</sub>	3.85 <sup>+0.06</sup> <sub>-0.06</sub>
HD 235858	2.8	2.73	5250 ± 125	5325 ± 250	3.94 <sup>+0.03</sup> <sub>-0.04</sub>	3.75 <sup>+0.04</sup> <sub>-0.03</sub>
IRAS 01259+6823	3.0	3.20	5500 ± 125	5510 ± 250	3.47 <sup>+0.04</sup> <sub>-0.04</sub>	2.53 <sup>+0.28</sup> <sub>-0.19</sub>
IRAS 12360-5740	2.7	3.10	7500 ± 125	7273 ± 250	3.88 <sup>+0.08</sup> <sub>-0.11</sub>	3.80 <sup>+0.10</sup> <sub>-0.09</sub>
V* LN Hya	1.0	0.93	6250 ± 125	6393 ± 250	4.02 <sup>+0.04</sup> <sub>-0.04</sub>	4.03 <sup>+0.04</sup> <sub>-0.03</sub>
V* V1401 Aql	1.0	1.24	6750 ± 125	6985 ± 250	3.47 <sup>+0.02</sup> <sub>-0.02</sub>	3.55 <sup>+0.02</sup> <sub>-0.01</sub>

**Notes.** <sup>(\*)</sup>Note the  $A(V)$  difference between both works, higher than 0.5 mag. Rao et al. (2012) did not find a C/O ratio greater than 1 nor  $s$ -process enrichment in HD 107369, as it is expected for an AGB star. In the present study, this star is classified as an unconfirmed post-AGB candidate. <sup>(1)</sup>Calculated by VOSA, <sup>(2)</sup>Kamath et al. (2022).

**Fig. 4.** Temperature distribution for the 118 stars for which we provide an SED fitting.

This procedure has allowed us to derive coherent pairs of temperature/total extinction and the luminosity for each of the 118 stars in our final working sample. The uncertainty values for the luminosity were estimated by VOSA using the uncertainties in the photometry and taking into account the distance uncertainties (lower and upper limits) that we provided as input. The VOSA software provides uncertainties in luminosity below 10% in general, which can be considered as a lower limit. As mentioned, VOSA does not support the use of errors in the extinction values to compute the SED fitting. More information about the fitting procedure is provided in Bayo et al. (2008) and in the VOSA documentation<sup>11</sup>.

This procedure, together with accurate distances from *Gaia* parallaxes, allowed us to obtain values for the luminosities and the total extinctions that agree, for instance, with those given by Kamath et al. (2022) as illustrated in Table 1. However, the fitting procedure we used to estimate the luminosity and temperature values has its own limitations because it does not take the uncertainty of the total extinction values into account

(which affects the luminosity uncertainties), and it also depends on the fitting models.

The VOSA tool fitting of Kurucz models also allowed us to obtain tentative values of  $\log[g]$  (which covers a range between 0 and 5) and metallicity (which covers a range between  $-4$  and  $0.5$ ) for our sample stars, although more reliable values for these parameters can be obtained from spectroscopy when available. In Tables A.6 and A.7 (available at the CDS) we provide the fitted SEDs for all the 118 objects in our final sample, including these parameters. The luminosity values together with lower and upper uncertainties, with the limitations explained before, are presented in Tables A.2–A.5.

Following Kamath et al. (2015), we analysed the shape of the SEDs and provide a classification into three different types (stellar, shell, or disc). This can give us some additional clues about the possible incidence of binarity in our sample. According to these authors, disc-type SEDs are related to binarity. We classified 30 SEDs as disc-type. The SED morphological classification for our objects is shown in Tables A.2–A.5. We opted to locate the disc-type SEDs in an HR diagram along with the remaining objects as their identification as binaries is tentative and not confirmed in general.

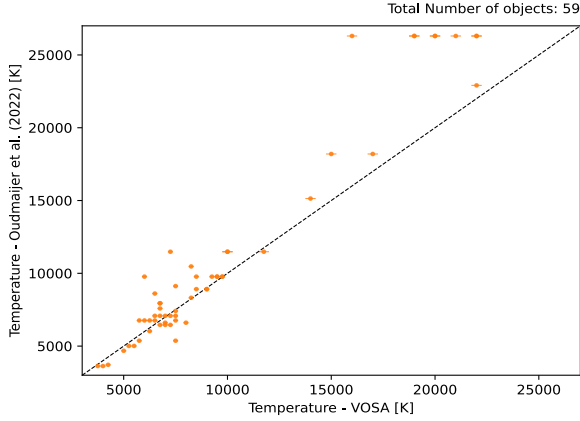
Figure 4 depicts the temperature distribution for our final sample of objects. Most stars (84%) have values below 10 000 K, as expected for post-AGB stars, and only three stars exhibit effective temperatures above 20 000 K. These last three are sources with infrared flux excess that have already started to ionise their envelopes on their way to the planetary nebula phase.

When we compare our temperature determinations with those obtained by Oudmaijer et al. (2022) for the 59 objects in common in both samples, we find (Fig. 5) that the temperatures in Oudmaijer et al. (2022) tend to be slightly higher than those we obtained. The mean difference is  $\langle \Delta T_{\text{eff}} \rangle = 1.55 \pm 0.78$  kK.

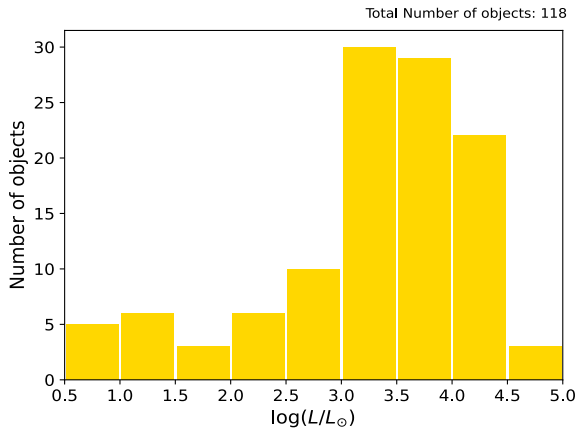
The temperatures in Oudmaijer et al. (2022) are based on spectral types collected from the Simbad database, which have very different origins and qualities. This might explain the discrepancies.

Figure 6 shows that the stellar luminosities of most of the candidate objects lie between  $2.5 < \log[\frac{L}{L_{\odot}}] < 4.5$ . This region

<sup>11</sup> <http://svo2.cab.inta-csic.es/theory/vosa/>



**Fig. 5.** Temperature values from our VOSA analysis vs. those from Oudmaijer et al. (2022) for the 59 objects in common with known temperature values.



**Fig. 6.** Luminosity distribution for the 118 stars in the final sample.

includes the main luminosity range expected for post-AGB stars, but the histogram includes a wide zone of underluminous objects as well.

Figure 7 shows the comparison between our luminosity values and those presented in Oudmaijer et al. (2022) for the 69 stars in common. Not all objects with a luminosity value in Oudmaijer et al. (2022) have a temperature value. The luminosity values from Oudmaijer et al. (2022) are very similar to those obtained in this work, the mean difference is  $< \Delta \text{Log}(L) > = 0.02 \pm 0.17$ .

Oudmaijer et al. (2022) determined their luminosities through the dereddened integrated fluxes obtained from Vickers et al. (2015) and by multiplying by the square of the distances from *Gaia* DR3 parallaxes. The authors indicated that the errors in the fluxes are about 20%, which could explain some differences. It is also important to note that Vickers et al. obtained their integrated fluxes assuming default values for the luminosity, which implies then that the values in Oudmaijer et al. (2022) were calculated using a rather circular argument.

The temperature and luminosity individual values for all of our objects are available in Cols. 6 and 8 of Tables A.2–A.5.

### 3.4. Galactic heights and membership to the halo

The precise *Gaia* DR3 distances allowed us to calculate the Galactic distribution of our final sample. Figure 8 depicts the Galactic height as a function of the Galactic longitude. It also

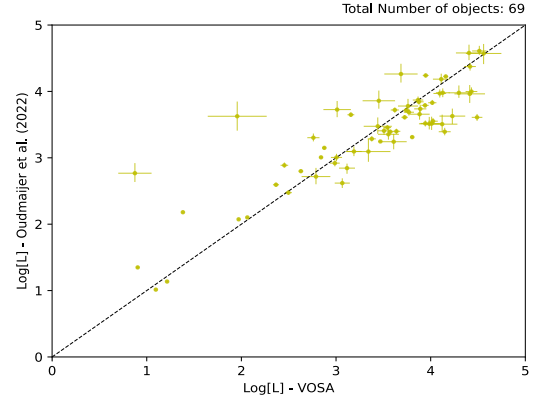


**Fig. 7.** Luminosity values from VOSA vs. those from Oudmaijer et al. (2022) for the 69 objects in common with known luminosity values.

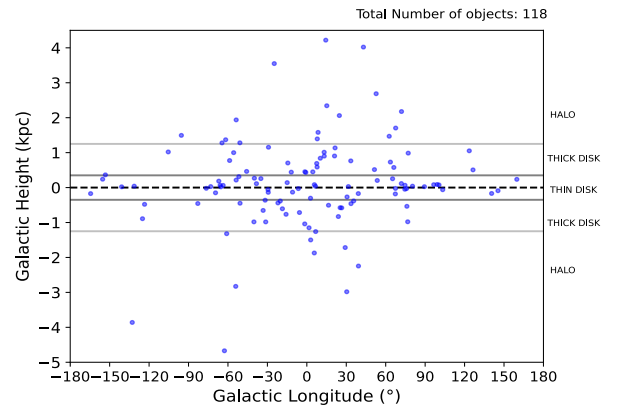


**Fig. 8.** Galactic height vs. Galactic longitude for all 118 post-AGB final sample candidates.

shows the commonly adopted limits for the main structures in the Milky Way: the thin disc, thick disc, and the halo.

This distribution allowed us to tentatively assign the 118 objects to either the 83 disc objects with  $z \leq 1.25$  kpc or to the halo (35). Suspected halo stars are flagged with ‘H’ in Tables A.2, A.3, and A.5. Although this classification was adopted to compare their position in the HR diagram with evolutionary tracks suited for each of the populations, we are well aware that it will benefit from a spectroscopic confirmation.

### 3.5. Classification: Identification of post-AGB stars and other objects

After the luminosity values and their uncertainties were known, we applied the luminosity thresholds discussed before. We obtained that 69 objects can be classified as post-AGB star bona fide candidates, 46 objects cannot be confirmed as post-AGB stars because we derived a luminosity lower than  $2500 L_{\odot}$  for them, and 3 objects above the high  $35000 L_{\odot}$  luminosity threshold are classified as supergiant stars.

In the sample of 46 stars with luminosities lower than  $2500 L_{\odot}$ , 5 are found to be YSOs in molecular clouds (see below), 3 are suspected or confirmed to be Horizontal Branch (HB) stars, and 38 remain unclassified. In this last group, 9 objects with luminosity lower than  $100 L_{\odot}$  are tentatively classified as possible YSOs, as we discuss below. The properties of the objects in the main categories are listed in Table A.2 (post-AGB stars), Table A.3 (unconfirmed post-AGB candidates),

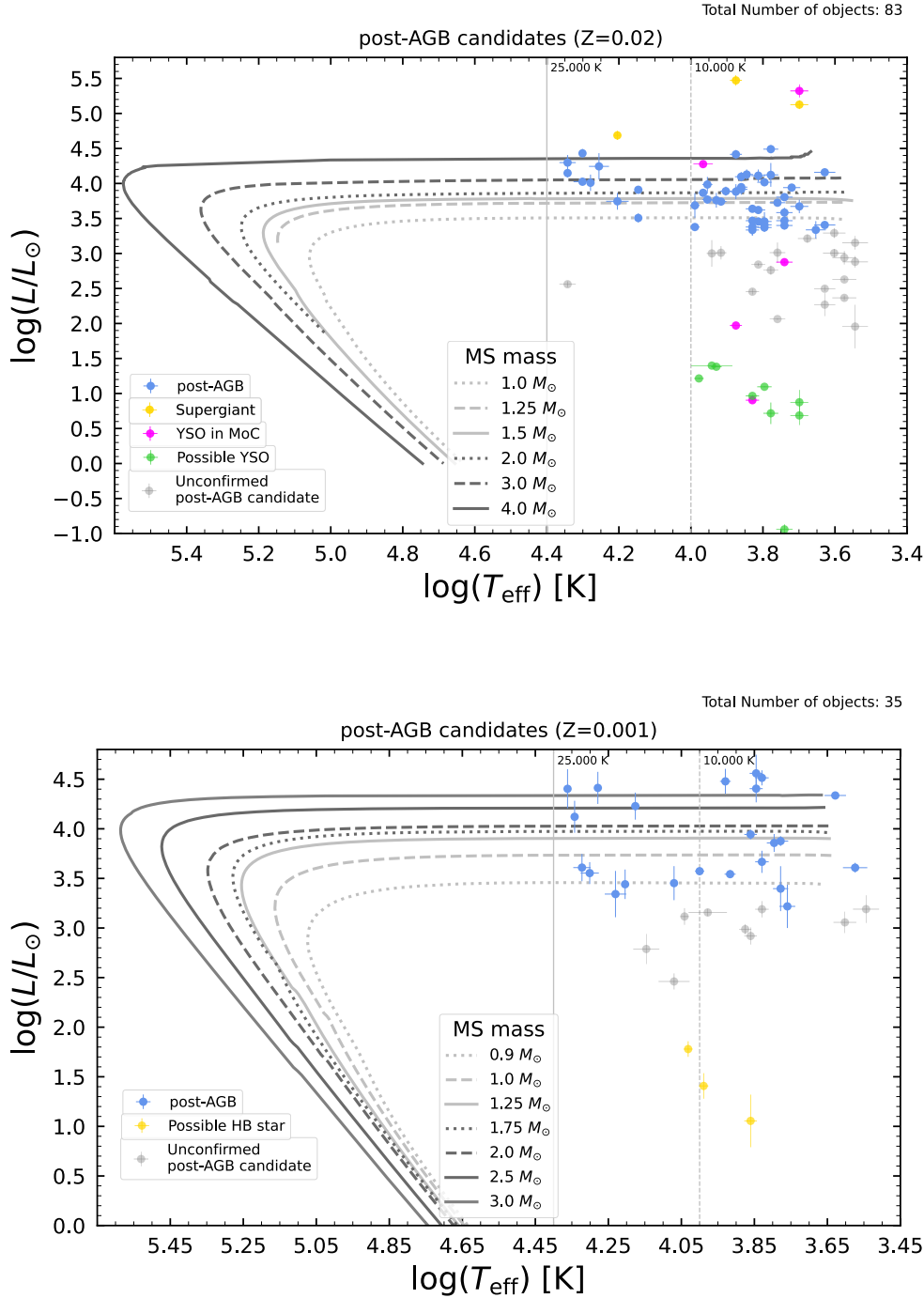


**Fig. 9.** Location in the HR Diagram of the 118 post-AGB candidates with luminosities and temperatures derived using VOSA. Evolutionary tracks by Miller Bertolami (2016) are shown and the objects are colour-coded according to the classification shown in the legend. The upper panel shows those objects located within the Galactic disc, with  $|z| \leq 1.25$  kpc, and  $Z = 0.02$  evolutionary tracks for comparison, while in the lower panel, those with  $|z| > 1.25$  kpc (Galactic halo) together with  $Z = 0.001$  tracks are shown.

Table A.4 (YSOs candidates), and Table A.5 (supergiants and HB stars).

To illustrate these results, we depicted all these objects in the HR diagram (Fig. 9) together with the evolutionary tracks for post-AGB stars and PNe central stars from Miller Bertolami (2016). To derive the masses, we used the tracks with a metallicity of  $z = 0.02$  for stars with  $z \leq 1.25$  kpc that are expected to be in the disc (upper panel), while for those with  $z > 1.25$  kpc, we used the  $z = 0.001$  tracks. With the luminosity threshold for post-AGB stars discussed before, the diagram allowed us to disclose bona fide post-AGB candidates from those that are not.

We would like to stress the fact that we applied a quite restrictive selection threshold to sort out bona fide post-AGB candidates. Some other objects that are located close to our

luminosity threshold might also be post-AGB, but given the uncertainties, they do not fulfil our selection criteria for possible post-AGB stars.

Twelve of the objects that we classified as post-AGBs have been identified as possible or confirmed binary stars by Kluska et al. (2019). We checked the bibliography for other binary references and found 5 additional binary stars. We identify these stars, together with two possible YSO binary stars, also according to Kluska et al. (2019), one supergiant star, and one post-AGB unconfirmed candidate with a flag in Table A.1. Moreover, our SED classification is disc-type for all but one of these binary objects.

Figure 9 also shows two types of YSOs. All objects with  $L < 100 L_{\odot}$  are suspected to be YSOs, but they might also be



other types of evolved stars, such as HB stars. There are also examples of well-known YSOs among the objects with higher luminosities. The physical nature of YSOs of these luminous objects is more difficult to discern because their luminosities and temperatures overlap with those of post-AGB stars. We studied their locations in the Galaxy. If their positions and distances matched those of star-forming regions, they were quite safely classified as young objects.

We used the molecular cloud catalogue by Zucker et al. (2020), which gives coordinates and distances to a large number of these regions. We found that five of our objects are located within these clouds. These objects are labelled “YSO in MoC” (molecular clouds) in Fig. 9 and Table A.4.

The luminosities of three of these objects are above  $L < 100 L_{\odot}$ , and the luminosities of two others are below this limit. The classification as a YSO of the remaining eight objects with luminosities below  $L < 100 L_{\odot}$  is tentative. We therefore label them possible YSOs in Fig. 9.

Figure 9 also shows three objects that we found to be Horizontal Branch stars: SDS2012 Ter8 38 is a blue Horizontal Branch star in the globular cluster Terzan 8, [SDS2012] NGC 6402 160 in NGC 6402 and BPS BS 16479-0009 is a field Horizontal Branch star candidate according to Beers et al. (1996). Finally, we found three objects above the upper luminosity limit expected for post-AGB stars that we classify as supergiant stars. We comment further on them in Sect. 5.

### 3.6. Comparison with other classifications in the literature

We can compare our classification with the classification recently obtained by Aoki et al. (2022) for the seven objects in common in both samples. Four post-AGBs are identically classified by both of us, while two of our unconfirmed post-AGB stars were catalogued as post-AGB or as cool post-AGB by them, and one of our possible YSOs was catalogued as a hot subdwarf by these authors.

When comparing our results with those in Kamath et al. (2022), we found 11 objects in common (those with good astrometric quality in that work, RUWE<1.4). We can confirm a nature as bona fide post-AGB candidates for 10 of these, while HD 107360 remains slightly underluminous for the post-AGB threshold. In general, the temperatures and luminosity values given by Kamath et al. (2022) agree with our derived values, as illustrated in Table 1.

In Sect. 3.3, we compared our results with those obtained by Oudmaijer et al. (2022), as shown in Figs. 5 and 7. For the luminosity range expected for post-AGB stars, the temperatures and luminosities agree with a dispersion that can be explained by methodological differences, as already discussed in that section. Forty-four of the 59 objects in common with Oudmaijer et al. (2022) sample were classified as post-AGB 44, and we catalogued 8 of them as unconfirmed candidates, 3 as possible YSOs, 2 as YSOs in molecular clouds, and another 2 as supergiants.

Finally, we summarise our results. Starting from the lists of post-AGB objects known or proposed as such in the literature, we selected stars based on the quality of the astrometry in *Gaia* DR3 of these sources. We used updated dust-extinction maps, 3D when available, to derive more accurate luminosities. As a consequence, we were able to classify some of them as bona fide post-AGB stars (69), supergiants (3), HB stars (3), YSOs in molecular clouds (5), and possible YSOs (9), while 29 objects remain unconfirmed post-AGB candidates. In the following section, we describe the evolutionary properties of our sample of 69 post-AGB stars.

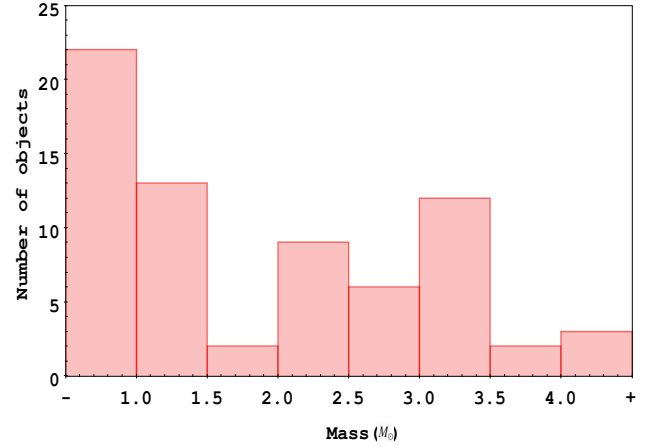


Fig. 10. Progenitor mass distribution for the 69 post-AGB objects.

## 4. Sample of post-asymptotic giant branch stars

We focus now on the sample of 69 objects whose luminosities allowed us to confirm their evolutionary state as bona fide post-AGB candidates. By interpolating between the novel evolutionary models by Miller Bertolami (2016) for post-AGB stars, we estimated their progenitor mass (in the MS) and their evolutionary age in the post-AGB phase. Miller Bertolami (2016) provided tracks for metallicity values 0.01, 0.02, 0.001, and 0.0001. We used the tracks for  $Z = 0.02$  as representative of the disc population, and for objects belonging to the halo, we used  $Z = 0.001$  tracks.

The objects classified as unconfirmed post-AGB candidates are located below the  $1 M_{\odot}$  track ( $0.9 M_{\odot}$  for halo stars). It is assumed that the initial masses of these objects, if they are single-evolved stars, can only be slightly below  $1 M_{\odot}$ . Conversely, they could have their origin in binary evolution.

The progenitor mass distribution we obtained for the post-AGB stars in our sample is displayed in Fig. 10. The masses of about half of our stars (35) are below  $1.5 M_{\odot}$  in the MS, and the masses of only 5 of them are higher than  $3.5 M_{\odot}$ . Although our study is limited in the number of objects and possibly comes from a biased selection, the resulting masses match the expected distribution. The lifetimes of parent stars with masses above  $3.5 M_{\odot}$  are too short in the post-AGB phase (the crossing times for post-AGB and PNe phases in Miller Bertolami tracks are shorter than 400 yr) for them to populate this region. The mean value of the progenitor masses for the post-AGB sample is

$$\langle M \rangle_{\text{MS}} = 1.94 \pm 0.53 M_{\odot}.$$

This mean mass value agrees with the value of  $1.8 \pm 0.5 M_{\odot}$  obtained in González-Santamaría et al. (2021) for stars in the next evolutionary phase, as central stars of planetary nebulae.

The mean mass value for the post-AGB stars final sample is

$$\langle M \rangle_{\text{postAGB}} = 0.598 \pm 0.163 M_{\odot}.$$

We obtained the evolutionary age distribution shown in Fig. 11. The ages of about 36% of the stars are younger than 2000 yr. Moreover, almost all the objects in the sample show evolutionary ages below 10 000 yr, and only 6 stars are older. We obtained the following mean evolutionary age of the sample:

$$\langle T \rangle_{\text{evo}} = 5.66 \pm 3.60 \text{ kyr}.$$

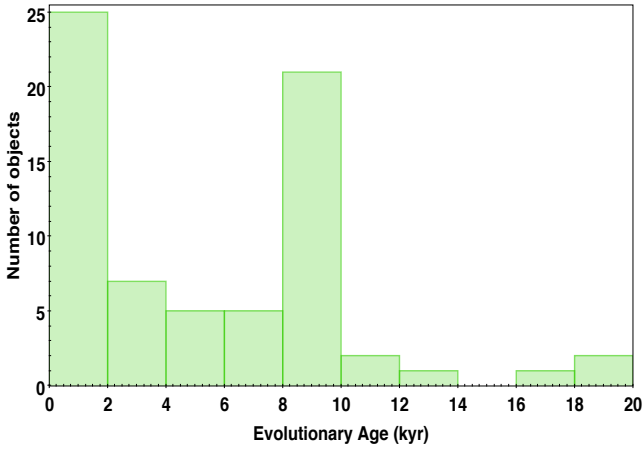


**Fig. 11.** Distribution of the evolutionary age for the 69 post-AGB objects.

In Miller–Bertolami models, the beginning of the post-AGB phase is taken when the mass of the external layer of the star drops below 1% of the star mass as a result of stellar winds.

Individual mass and evolutionary age values can be found in Cols. 11 and 12 of Table A.2, respectively.

## 5. Special objects

Our study allows us to confirm the nature of three objects as post-AGB stars. They lacked a previous firm classification in the catalogues and were neither listed in the Torun catalogue as likely, nor in Simbad or in the Suárez et al. catalogues as confirmed post-AGB.

CD-30 15464. This object is catalogued as possible post-AGB in the Torun catalogue but as simple star in Simbad, and it has no references in Suárez et al. (2006) catalogue. It is reported as a star of spectral type B1, while its effective temperature is quite high (22 000 K), still within the limits of a post-AGB star. It is located very far from the Sun, at a distance of 9.96 kpc, in the direction of the Galactic centre ( $l = 1.67^\circ$ ) and slightly below the Galactic disc ( $b = -6.63^\circ$ ). Despite this location, the interstellar extinction is low in the direction of this star ( $A_V = 0.75$ ), and its image<sup>12</sup> in PanSTARRS colours shows evidence of a circumstellar envelope.

HD 53300 is catalogued as an A2 type star and is located in the Galactic disc ( $b = 0.44^\circ$ ). Instead, Rao et al. (2012) derived an effective temperature of 7250 K for it, which corresponds to an F1 type star. This star is mentioned as a candidate post-AGB in the Simbad database and lacks references in the Torun or Suárez et al. (2006) catalogues, although Rao et al. (2012) classified it as post-AGB star, while it was classified in Bhatt & Manoj (2000) as a Vega-like star.

HD 214539. This star is catalogued as possible post-AGB in Torun and as simple star in Simbad, with a spectral type B8/9. Kodaira & Philip (1984) obtained a temperature of 10 000 K and a gravity of  $\log[g]=2$  for this object. It is located at a distance of 1.39 kpc. By visual inspection<sup>13</sup>, a circumstellar envelope typical of post-AGB stars can also be observed.

It is also interesting to analyse the three highly luminous objects ( $\log[\frac{L}{L_\odot}] > 4.5$ ) that we have catalogued as supergiant stars.

BD-02 4931. This object is catalogued as a post-AGB candidate star in the Simbad database, while in Parthasarathy et al. (2000a), it is classified as a B1 type giant. Assuming a temperature of 16 000 K from its spectral type (the same value as was obtained by fitting its SED by Gielen et al. 2011), we obtained a luminosity of  $\log[\frac{L}{L_\odot}] = 4.69$ , which is higher than the predictions for post-AGB stars.

HD 179821. This star is catalogued as likely post-AGB in the Torun catalogue and as a post-AGB star in the Simbad database and in the Suárez et al. catalogue. However, we obtained a high luminosity of  $\log[\frac{L}{L_\odot}] = 4.75$  (very similar to that obtained by Wood et al. 1983,  $\log[\frac{L}{L_\odot}] = 4.7$ ) and low surface gravity of  $\log[g] = 0.5$  for this object, which led us to classify it as a supergiant star. Moreover, Şahin et al. (2016) catalogued it as a likely massive post-red supergiant star.

V\* V1027 Cyg. This object is also classified as likely post-AGB in the Torun catalogue and as post-AGB in Simbad database. In this case, however, we obtained stellar parameters typical of supergiant stars, such as a high luminosity of  $\log[\frac{L}{L_\odot}] = 4.75$  and a very low surface gravity of  $\log[g] = 0$ . Furthermore, in the Winfrey et al. (1994) catalogue, they classified it as a G7 supergiant star, but it was catalogued as a G8-K3 type supergiant in a more recent study by Arkhipova et al. (2016).

## 6. Conclusions

Based on a sample of 118 post-AGB star candidates selected from the literature and after filtering out stars for which *Gaia* DR3 astrometry was not accurate enough (and for which the distances were therefore unreliable), we have estimated their luminosity values, which allowed us to classify them as bona fide post-AGB candidates (69) or as objects in a different evolutionary phase, such as YSOs (5), possible YSOs (9), supergiant stars (3), and HB stars (3). Twenty-nine stars remain unconfirmed post-AGB candidates.

Using the Spanish VOSA service, we fitted the SEDs of each star and simultaneously obtained its effective temperature and luminosity. This allowed us to plot the post-AGB candidates in an HR diagram, and by using the Miller Bertolami (2016) evolutionary tracks in the post-AGB phase, we derived their masses and ages. We found that our 69-object sample includes mainly stars with progenitor masses between 1 and 2.5  $M_\odot$ , which agree with the type of post-AGB stars that statistically could be found in a small sample like ours. The mass mean value of the sample also agrees with that expected for stars in the planetary nebula phase (the next evolutionary phase) according to González-Santamaría et al. (2021).

Our study allowed us to confirm the nature of several objects as post-AGB stars that were previously not confirmed as such. It is important to note that although the *Gaia* DR3 catalogue contains statistically valuable information for an enormous number of stars, many of the available parallaxes contain errors that are too large to allow a correct estimation of the absolute magnitude or luminosity of the stars. We chose to perform a rather restrictive filtering of the astrometric quality of *Gaia* measurements (parallax and distance errors, RUWE value) as well as of the distance inferred from the parallax measurement by a Bayesian model of Galactic stellar distributions.

This filtering was based on the idea of working with a small set of objects, candidates for the post-AGB phase, all of which have precise distances in *Gaia*, which therefore mostly are individual objects for which a luminosity can be calculated with great confidence. For this reason, our method was based on

<sup>12</sup> <http://cdsportal.u-strasbg.fr/?target=CD-30%2015464>

<sup>13</sup> <http://cdsportal.u-strasbg.fr/?target=HD%20214539>

selecting only a subset of stars that are firm candidates to be in the post-AGB phase and have *Gaia* DR3 parallaxes (and inferred distances) with errors below 30%.

We also only worked with candidates with interstellar extinction values from Stassun 3D dust maps, which allowed us to initially constrain interstellar extinction. The total extinction, including both interstellar and circumstellar extinction, was derived simultaneously with the luminosity value from the SED-fitting procedure. The effective temperatures were taken from the literature, using spectroscopically determined temperatures when they were available.

We discussed our results in comparison with other similar studies of post-AGBs that were carried out recently. About 25% of the stars in our sample are too underluminous to be confirmed as post-AGB stars under our working hypotheses, while 12% are found to be possible YSOs, are either located in Molecular Clouds (5) or are candidates (9). Other objects, such as HB stars (3) or supergiant stars (3), were also included in the original compilation.

Although our initial filtering would rule out most of the binary objects, we found that the SEDs of 18 objects out of our sample of 69 post-AGB can be classified as disc-type. They might therefore be binary objects. Searching the literature for binarity, we found that 17 of these objects were identified as such either by Kluska et al. (2022) (12 objects) or by other authors (see Table A.1 for references). This means that our sample contains 18 possible or confirmed binaries, which is about 26%.

Our results provide an interesting framework for further insight into the post-AGB phase. In particular, our well-characterised sample of 69 objects opens the way to complementing the study on the unconfirmed 29 candidates. A follow-up analysis of their properties, including spectroscopy when possible, would be desirable.

**Acknowledgements.** This work has made use of data from the European Space Agency (ESA) *Gaia* mission, processed by the *Gaia* Data Processing and Analysis Consortium (DPAC). Funding for the DPAC has been provided by national institutions, in particular, the institutions participating in the *Gaia* Multilateral Agreement. This research has made use of the Simbad database and the Aladin sky atlas, operated at CDS, Strasbourg, France. The authors have also made use of the VOSA software, developed under the Spanish Virtual Observatory project supported by the Spanish MINECO through grant PID2020-112949GB-I00, and partially funded by the European Union's Seventh Framework Programme (FP7-SPACE-2013-1) for research, technological development and demonstration under grant agreement no. 60674. This research was funded by the Spanish Ministry of Science MCIN / AEI / 10.13039 / 501100011033 and the European Union Next Generation programme EU/PRTR through the coordinated grant PID2021-122842OB-C22 and the Horizon Europe [HORIZON-CL4-2023-SPACE-01-71] SPACIOUS project, Grant Agreement no. 101135205. Additionally, it is co-financed by the EU through the FEDER Galicia 2021-27 operational programme, Ref. ED431G 2023/01. E.V. acknowledges support from the 'DISCOBOLO' funded by the Spanish Ministerio de Ciencia, Innovación y Universidades under grant PID2021-127289NB-I00. M.M. and E.V. acknowledge support from the cooperation agreement between the IAC and the Fundación Jesús Serra for visiting grants. AM acknowledges support from the ACIISI, Gobierno de Canarias and the European Regional Development Fund (ERDF) under grant with reference PROID2020010051 as well as from the State Research Agency (AEI) of the Spanish Ministry of Science and Innovation (MICINN) under grant PID2020-115758GB-I00.

## References

Aoki, W., Matsuno, T., & Parthasarathy, M. 2022, *PASJ*, 74, 1368  
 Arentsen, A., Prugniel, P., Gonneau, A., et al. 2019, *A&A*, 627, A138  
 Arhipova, V. P., Taranova, O. G., Ikonnikova, N. P., et al. 2016, *Astron. Lett.*, 42, 756

Bailer-Jones, C. A. L., Rybizki, J., Foesneau, M., Demleitner, M., & Andrae, R. 2021, *AJ*, 161, 147  
 Bayo, A., Rodrigo, C., Barrado Y Navascués, D., et al. 2008, *A&A*, 492, 277  
 Beers, T. C., Wilhelm, R., Doinidis, S. P., & Mattson, C. J. 1996, *ApJS*, 103, 433  
 Bhatt, H. C., & Manoj, P. 2000, *A&A*, 362, 978  
 Bloeker, T. 1995, *A&A*, 299, 755  
 Bonnarel, F., Fernique, P., Bienaymé, O., et al. 2000, *A&AS*, 143, 33  
 Buder, S., Sharma, S., Kos, J., et al. 2021, *MNRAS*, 506, 150  
 Castelli, F., & Kurucz, R. L. 2003, in *Modelling of Stellar Atmospheres*, 210, eds. N. Piskunov, W. W. Weiss, & D. F. Gray, A20  
 Corporaal, A., Kluska, J., Van Winckel, H., et al. 2023, *A&A*, 674, A151  
 de Ruiter, S., van Winckel, H., Dominik, C., Waters, L. B. F. M., & Dejonghe, H. 2005, *A&A*, 435, 161  
 Doroshenko, V., Pühlhofer, G., Kavanagh, P., et al. 2016, *MNRAS*, 458, 2565  
 Drilling, J. S., Jeffery, C. S., Heber, U., Mochler, S., & Napiwotzki, R. 2013, *A&A*, 551, A31  
 Dubus, G., Otulakowska-Hypka, M., & Lasota, J.-P. 2018, *A&A*, 617, A26  
 Fabricius, C., Luri, X., Arenou, F., et al. 2021, *A&A*, 649, A5  
 Firnstein, M., & Przybilla, N. 2012, *A&A*, 543, A80  
 Fitzpatrick, E. L. 1999, *PASP*, 111, 63  
 Gallardo Cava, I., Alcolea, J., Bujarrabal, V., Gómez-Garrido, M., & Castro-Carrizo, A. 2023, *A&A*, 671, A80  
 Garcia-Lario, P., Manchado, A., Pych, W., & Pottasch, S. R. 1997, *A&AS*, 126, 479  
 Gielen, C., Bouwman, J., van Winckel, H., et al. 2011, *A&A*, 533, A99  
 Gonzalez, G., & Wallerstein, G. 1992, *MNRAS*, 254, 343  
 González-Santamaría, I., Manteiga, M., Manchado, A., et al. 2021, *A&A*, 656, A51  
 Hardorp, J., Theile, I., & Voigt, H. H. 1965, *Hamburger Sternw. Warner & Swasey Obs.*, C05, 0  
 Henize, K. G. 1976, *ApJS*, 30, 491  
 Herrero, A., Parthasarathy, M., Simón-Díaz, S., et al. 2020, *MNRAS*, 494, 2117  
 Hunger, K., & Kaufmann, J. P. 1973, *A&A*, 25, 261  
 Ikonnikova, N. P., Parthasarathy, M., Dodin, A. V., Hubrig, S., & Sarkar, G. 2020, *MNRAS*, 491, 4829  
 Indebetouw, R., Mathis, J. S., Babler, B. L., et al. 2005, *ApJ*, 619, 931  
 Jeffery, C. S. 1993, *A&A*, 279, 188  
 Jeffery, C. S., Hamill, P. J., Harrison, P. M., & Jeffers, S. V. 1998, *A&A*, 340, 476  
 Kamath, D., Wood, P. R., & Van Winckel, H. 2015, *MNRAS*, 454, 1468  
 Kamath, D., Van Winckel, H., Ventura, P., et al. 2022, *ApJ*, 927, L13  
 Klochkova, V. G. 2014, *Astrophys. Bull.*, 69, 279  
 Klochkova, V. G., & Chentsov, E. L. 2018, *Astron. Rep.*, 62, 19  
 Klochkova, V. G., Sendzikas, E. G., & Chentsov, E. L. 2018, *Astrophys. Bull.*, 73, 52  
 Kluska, J., Van Winckel, H., Hillen, M., et al. 2019, *A&A*, 631, A108  
 Kluska, J., Van Winckel, H., Coppée, Q., et al. 2022, *A&A*, 658, A36  
 Kodaira, K., & Philip, A. G. D. 1984, *ApJ*, 278, 208  
 Kwok, S. 2000, *The origin and evolution of planetary nebulae*. Camb. Astrophys. Ser., 33  
 Lada, C. J., Muench, A. A., Luhman, K. L., et al. 2006, *AJ*, 131, 1574  
 Lindegren, L., Hernández, J., Bombrun, A., et al. 2018, *A&A*, 616, A2  
 Lindegren, L., Bastian, U., Biermann, M., et al. 2021, *A&A*, 649, A4  
 Luck, R. E. 2014, *AJ*, 147, 137  
 Maas, T., Van Winckel, H., & Lloyd Evans, T. 2005, *A&A*, 429, 297  
 Mello, D. R. C., Daflon, S., Pereira, C. B., & Hubeny, I. 2012, *A&A*, 543, A11  
 Miller Bertolami, M. M. 2016, *A&A*, 588, A25  
 Mooney, C. J., Rolleston, W. R. J., Keenan, F. P., et al. 2004, *A&A*, 419, 1123  
 Napiwotzki, R., Heber, U., & Koepfen, J. 1994, *A&A*, 292, 239  
 Oomen, G.-M., Van Winckel, H., Pols, O., et al. 2018, *A&A*, 620, A85  
 Oudmaijer, R. D., Jones, E. R. M., & Vioque, M. 2022, *MNRAS*, 516, L61  
 Parthasarathy, M., Sivarani, T., Garcia-Lario, P., & Manchado, A. 2000a, *AAS Meet. Abstr.*, 197, 60.05  
 Parthasarathy, M., Vijapurkar, J., & Drilling, J. S. 2000b, *A&AS*, 145, 269  
 Parthasarathy, M., Matsuno, T., & Aoki, W. 2020, *PASJ*, 72, 99  
 Parthasarathy, M., Kounkel, M., & Stassun, K. G. 2022, *RNAAS*, 6, 171  
 Quin, D. A., & Lamers, H. J. G. L. M. 1992, *A&A*, 260, 261  
 Raman, V. V., Anandarao, B. G., Janardhan, P., & Pandey, R. 2017, *MNRAS*, 470, 1593  
 Rao, S. S., Giridhar, S., & Lambert, D. L. 2012, *MNRAS*, 419, 1254  
 Reymiers, M., & Van Winckel, H. 2001, *A&A*, 365, 465  
 Şahin, T. 2018, *Astrophys. Bull.*, 73, 211  
 Şahin, T., Lambert, D. L., Klochkova, V. G., & Panchuk, V. E. 2016, *MNRAS*, 461, 4071

- Stassun, K. G. 2019, VizieR Online Data Catalog: [IV/38](#)
- Steinmetz, M., Guiglion, G., McMillan, P. J., et al. 2020, [AJ](#), **160**, 83
- Suárez, O., García-Lario, P., Machado, A., et al. 2006, [A&A](#), **458**, 173
- Szczerba, R., Siódmiak, N., Stasińska, G., & Borkowski, J. 2007, [A&A](#), **469**, 799
- Szczerba, R., Siódmiak, N., Stasińska, G., et al. 2012, [IAU Symp.](#), **283**, 506
- Taylor, M. B. 2005, [ASP Conf. Ser.](#), **347**, 29, Astronomical Data Analysis Software and Systems XIV, eds. P. Shopbell, M. Britton, & R. Ebert
- Ting, Y.-S., Conroy, C., Rix, H.-W., & Cargile, P. 2019, [ApJ](#), **879**, 69
- van Aarle, E., van Winckel, H., Lloyd Evans, T., et al. 2011, VizieR Online Data Catalog: [J/A+A/530/A90](#)
- Van Winckel, H. 1997, [A&A](#), **319**, 561
- Van Winckel, H., Jorissen, A., Exter, K., et al. 2014, [A&A](#), **563**, A10
- Vassiliadis, E., & Wood, P. R. 1993, [ApJ](#), **413**, 641
- Venn, K. A., Smartt, S. J., Lennon, D. J., & Dufton, P. L. 1998, [A&A](#), **334**, 987
- Vickers, S. B., Frew, D. J., Parker, Q. A., & Bojčić, I. S. 2015, [MNRAS](#), **447**, 1673
- Villaver, E., Machado, A., & García-Segura, G. 2002, [ApJ](#), **581**, 1204
- Waelkens, C., Van Winckel, H., Bogaert, E., & Trams, N. R. 1991, [A&A](#), **251**, 495
- Wallerstein, G. 1958, [ApJ](#), **127**, 583
- Weidmann, W. A., Mari, M. B., Schmidt, E. O., et al. 2020, [A&A](#), **640**, A10
- Winfrey, S., Barnbaum, C., Morris, M., & Omont, A. 1994, [AAS Meet. Abstr.](#), **185**, 45.15
- Wood, P. R., Bessell, M. S., & Fox, M. W. 1983, [ApJ](#), **272**, 99
- Zucker, C., Speagle, J. S., Schlafly, E. F., et al. 2020, [A&A](#), **633**, A51

## Appendix A: Data Tables

Table A.1. General data of the 157 post-AGB candidates.

Num	Simbad Name	<i>Gaia</i> EDR3 ID	RA ( $^{\circ}$ )	Dec ( $^{\circ}$ )	G mag	$A_V^{IS}$	Spectral Type	Reference	Flag
1	* 42 Cyg	2056972679739120000	307.335	36.4547	5.74	1.52	A2Iab-Ib	1	-
2	* 89 Her	4582795323914832000	268.8549	26.05	5.35	0.17	F2Ibp	1/2	B(1,2,3)
3	[SDS2012] NGC 6284 116	4112726164275562496	256.1875	-24.55	16.93	-	-	1	-
4	[SDS2012] NGC 6402 160	4368932547017571584	264.1583	-3.3867	16.85	1.64	-	1	-
5	[SDS2012] Ter 8 38	6741750932641613952	295.42	-34.0664	15.09	0.41	-	1	-
6	2MASS J00235767-7205296	4689637789379454848	5.9903	-72.0916	11.09	0.09	-	1	-
7	2MASS J01302276-7303339	4686479648370453760	22.5949	-73.0594	10.63	0.12	B	1/2	-
8	2MASS J05241036-2429206	2957941232276476800	81.0432	-24.4891	12.09	0.09	-	1	-
9	2MASS J06544616-1048325	3049274119844532224	103.6924	-10.8091	12.05	2.03	OB+	1	R(1)
10	2MASS J13272898-4722472	6083708479176016128	201.8708	-47.3798	13.09	0.37	-	1/2	R(1)
11	2MASS J14034398-6937097	5846979777414443264	210.9333	-69.6194	16.39	0.79	-	1	-
12	2MASS J16570924-0404243	4365635249084745600	254.2886	-4.0734	13.49	0.79	B	1	R(1)
13	2MASS J17390218-4500388	5955201232284272384	264.7591	-45.0108	13.01	1.15	-	1/2	R(1)
14	2MASS J17442550-1937537	4119884023727270272	266.1063	-19.6316	12.43	1.67	OB+	1	-
15	2MASS J18224265-3014383	4046476465531783424	275.6777	-30.244	11.8	0.39	B7Ib	1/2	-
16	2MASS J18530579-0842378	4203848980711226112	283.2741	-8.7105	13.14	1.14	-	1/2	-
17	BD+32 2754	1324742534573959424	249.0487	32.4893	9.47	0.07	F8	2	-
18	BD+33 2642	1369896865785991424	237.9995	32.9484	10.79	0.08	B2 IVp	1/2	B(4)
19	BD+48 1220	255225480926107392	76.9595	48.4026	9.53	0.89	A4Ia	1/2	-
20	BD-02 4931	4213102543594938880	289.5947	-2.703	10.42	1.68	B1III	1	B(5)
21	BD-13 5550	6879196723703009920	300.4576	-12.6883	11.34	0.44	B1Iae	1/2	-
22	BPS BS 16479-0009	3939536182204010880	198.4999	18.5253	13.61	0.06	-	1	-
23	CD-24 13065	4113478337639987200	256.0433	-24.4661	11.08	0.47	B8	1	-
24	CD-30 15464	4049379725984965120	274.002	-30.7565	11.9	0.75	B1Ib	2	-
25	CD-42 8141	6135778223095320960	197.1931	-43.4642	10.45	0.34	B2I	1	-
26	CD-46 11775	5948818331093816448	265.6416	-46.9802	11.17	0.61	OB+	1	-
27	CD-48 11445	5938738764416910848	256.9027	-48.319	10.5	2.24	G2p(R)	1	B(1,5)
28	CD-49 8217	6093466301247487488	207.3233	-50.3793	10.82	0.61	B2I	1	R(1)
29	CD-49 11554	5946845601071213696	263.7604	-49.4407	10.93	0.61	B3Ie	1/2	-
30	CD-53 5736	5893945588395282304	223.1197	-54.2952	10.87	2.53	A0Ie	1/2/3	-
31	CD-54 5573	5896479309853592448	212.6621	-55.0075	10.29	1.47	A3I	1/2/3	-
32	CD-54 6746	5932016212933920384	246.1642	-54.6357	9.45	1.11	B8Iab	1/2	-
33	CD-55 5174	6063703586653222144	202.4626	-56.1149	10.71	1.26	B1Iae	1/2/3	-
34	CD-59 6142	583129599979910656	246.2609	-60.059	9.98	0.59	A3Ie	1/2/3	-
35	CI* NGC 6779 SAW V6	2039259886717168896	289.1491	30.1941	12.53	0.56	kF5hF8	1	-
36	EM* GGR 44	2005246464463628800	331.0513	53.0671	12.43	1.11	B1I	1/2	R(1)
37	EM* SIHA 161	2049984454412871296	290.4804	35.0486	11.31	0.27	Fe	1/2/3	-
38	EM* VES 351	2168803045330976768	314.7316	49.5203	11.18	2.06	F3Ie	1/2/3	-
39	HD 53300	3101342596792542464	106.0812	-5.3054	7.94	0.98	A2II	1	-
40	HD 56126	3156171118495247360	109.0427	9.9967	8.1	0.08	F0/5Ia	1/2/3	-
41	HD 93662	5351069693654349952	161.9101	-57.4674	5.66	0.37	K5	1/2	B(1,2)
42	HD 101584	5343168568718268800	175.245	-55.5738	6.92	0.82	F0Iape	1/2	B(1,2,8)
43	HD 105262	3920735495441657728	181.7951	-12.9855	7.07	0.05	B9 Ibp	1/2	B(8)
44	HD 107369	3469106382752903168	185.1873	-32.5573	9.54	0.21	A2II/III	1/2	-
45	HD 108015	6130448958959242240	186.2229	-47.1521	7.86	0.31	F3/5Ib/II	1/2	B(1,2)
46	HD 116745	6083719439934104832	201.6097	-47.2743	10.68	0.36	F0Ibp	1/2	-
47	HD 133656	5903310335089068416	226.8643	-48.2983	7.49	0.74	A1/A2Ib/II	1/2/3	-
48	HD 144941	6042510190769087744	242.3523	-27.2273	10.09	0.72	B8	1	-
49	HD 148743	4351018375858237952	247.6251	-7.5145	6.37	0.67	A7Ib	1/2	-
50	HD 157350	4122877783340594176	260.8558	-17.971	8.56	0.1	A2III/IV	1	-
51	HD 161796	1367102319545324288	266.2311	50.0443	7.2	0.11	F3Ib	1/2/3	-
52	HD 167402	4049624646596488576	274.0779	-30.1249	8.94	0.73	O9.5/B0Ib/II	1	R(1)
53	HD 172324	2096072103492979584	279.4949	37.4349	8.16	0.11	A0Iabe	1/2	-
54	HD 172481	4072427555640528000	280.404	-27.9503	8.84	0.65	F2/3Ia	1/2	B(1,2)
55	HD 177566	6715619076008049792	286.7829	-41.7211	10.14	0.26	B6Ib	1/2	R(1)
56	HD 179821	4264026012336768000	288.4942	0.1255	7.55	1.25	G4 <sub>0</sub> - Ia	1/2/3	-
57	HD 186438	2049034819957965312	295.7205	37.6782	7.83	0.26	F3Ib	1/2	-
58	HD 187885	6871175064823382912	298.2196	-17.0307	8.48	0.62	F0Ie	1/2/3	-
59	HD 214539	6385794694664872320	340.1999	-67.6886	7.2	0.09	B8/9I	2	-
60	HD 235858	2006425553228658816	337.2933	54.8517	8.2	0.48	G5Ia	1/2	-
61	HD 246299	3336558507975208448	85.2377	10.2403	10.27	0.58	G2I	1/2/3	-
62	HD 306753	5335709477519159936	174.4288	-60.8976	12.36	2.01	A0	1/2	-
63	IRAS 01005+7910	565507868441719424	16.1896	79.4462	10.96	0.42	B2Iab	1/2/3	-
64	IRAS 01259+6823	532078488712794624	22.3892	68.6547	11.81	2.74	F5Ie	1/2	-
65	IRAS 02528+4350	433515788197481984	44.0473	44.0478	10.75	0.34	A0e	1/2	-
66	IRAS 07227-1320	3032030620730261376	111.2628	-13.4389	11.6	0.66	MII	2	-
67	IRAS 07582-4059	5534265613756612224	119.9905	-41.1231	14.55	2.5	-	2/3	R(2)
68	IRAS 08242-3828	5540178478053582592	126.5158	-38.6465	12.03	-	-	1/2	-
69	IRAS 08275-6206	5277809440015969792	127.1014	-62.2724	10.8	0.69	-	1/2	-
70	IRAS 08351-4634	5521628033275348480	129.19	-46.7469	17.13	1.64	-	1/2	R(3)
71	IRAS 09370-4826	5409357863031443840	144.728	-48.6731	13.75	0.41	-	2	R(3)
72	IRAS 11387-6113	5335675087769798272	175.2863	-61.5048	11.4	1.41	A3Ie	1/2/3	-
73	IRAS 11531-6111	5335102207846402176	178.9084	-61.4713	14.49	2.65	-	2	-
74	IRAS 12145-5834	6071416385848395008	184.3171	-58.8582	15.09	2.55	B8Ie	2	R(4)
75	IRAS 12360-5740	6060828565581083264	189.7213	-57.9422	12.08	1.62	-	1/2	-
76	IRAS 13110-6629	5857811238294426752	198.6128	-66.7594	10.54	-	-	1/2	-
77	IRAS 13356-6249	5865398796206273152	204.7763	-63.079	15.8	-	-	1/2	-
78	IRAS 13421-6125	5865808020691983104	206.392	-61.6677	16.18	5.47	-	2	R(3)
79	IRAS 14527-6204	5874676853324862720	224.1857	-62.2815	11.08	1.74	-	2	R(5)

Table A.1. Continued on next page.

Num	Simbad Name	Gaia EDR3 ID	RA ( $^{\circ}$ )	Dec ( $^{\circ}$ )	G mag	$A_V^{LS}$	Spectral Type	Reference	Flag
80	IRAS 15066-5532	5886573569080505216	227.6111	-55.7367	14.57	5.55	-	1/2	-
81	IRAS 16086-5255	5933063252888145920	243.1269	-53.0528	13.15	3.28	-	1/2	-
82	IRAS 16115-5044	5935061172876722176	243.8248	-50.8721	14.83	-	-	2	-
83	IRAS 16476-1122	4334241408966611328	252.6012	-11.466	11.09	1.7	M1I	2	-
84	IRAS 16494-3930	5969973999973524224	253.233	-39.5818	16.73	1.83	G2I	1	-
85	IRAS 16594-4656	5963059480546004608	255.792	-47.0077	14.6	-	-	1/2	-
86	IRAS 17208-3859	5972489407685976320	261.0812	-39.0294	15.46	2.45	-	2	-
87	IRAS 17223-2659	4109553493474085504	261.361	-27.0337	15.14	4.36	-	2	-
88	IRAS 17287-3443	5975119332093959552	263.0201	-34.7591	12.92	4.53	-	2	B(6)
89	IRAS 17310-3432	4053542580087893376	263.585	-34.5815	15.77	3.16	-	2	R(1)
90	IRAS 17332-2215	4117592469707529856	264.0712	-22.2889	15.22	2.27	-	2	-
91	IRAS 17364-1238	4161796857143755264	264.8205	-12.6749	12.8	1.76	-	2	-
92	IRAS 17433-1750	4120632688077368192	266.5659	-17.8628	13.33	1.64	M2I	1/2	R(3)
93	IRAS 17543-3102	4044070253255414656	269.39	-31.051	14.84	-	-	2	-
94	IRAS 17579-3121	4043901443659288448	270.3057	-31.3657	11.2	-	-	1/3	-
95	IRAS 17581-2926	4062288993280721792	270.314	-29.4441	11	1.59	-	2	R(5)
96	IRAS 18084-1737	4095941436385621888	272.8678	-17.611	15.71	1.07	G3I	1	R(4)
97	IRAS 18113-2503	4065347387968755328	273.6136	-25.0501	15.07	3.01	-	1/2	R(3)
98	IRAS 18158-3445	4044520262548753152	274.8057	-34.7417	12.45	0.42	F6	1	B(7)
99	IRAS 18435-0052	4260301176152524032	281.5326	-0.8114	10.93	3.28	B2II	2	-
100	IRAS 19075+0432	4293369057089082112	287.4997	4.619	14.44	4.79	-	1/2	-
101	IRAS 19225+3013	2038872686817523072	291.1122	30.3241	12.24	0.67	M2II	2	-
102	IRAS 19454+2920	2031794791233840128	296.8534	29.4697	15.29	4.43	C-rich	1/2	-
103	IRAS 20094+3721	2060806470651334912	302.82	37.5145	10.63	1.24	-	1/2	B(7)
104	IRAS 20174+3222	2054521833963867008	304.8659	32.5376	15.26	-	-	1/2	-
105	IRAS 20244+3509	2056435602670418688	306.6049	35.3204	13.97	5.34	-	1/2	-
106	IRAS 20259+4206	2068126263125039488	306.9261	42.2789	13.54	1.32	-	2	-
107	IRAS 20490+5934	2193902559325301760	312.5566	59.7642	10.37	0.63	A3e	1/2	-
108	IRAS 21289+5815	2179471159976791168	322.5951	58.4811	14.46	1.35	A2Ie	1/2	-
109	IRAS 21525+5643	2198987491374918528	328.5631	56.957	16.69	2.53	-	2	-
110	LB 3193	4715635535640762240	19.7214	-61.9281	12.66	0.05	-	1/2	-
111	LS IV -04 1	4365451214021224320	254.1155	-4.7899	12	0.86	B	1/2	-
112	LS IV -15 3	4136944866387751552	260.7996	-15.6209	11.76	1.21	A0Ie	1/2/3	-
113	LS 4331	4124125282361429504	265.2502	-16.3035	13.08	1.39	B1Ibe	1/2	-
114	LS 5112	4099619470274753408	280.2026	-17.0773	11.88	1.32	B1IIIep	1/2	-
115	LS II +34 26	1869422453048750336	312.0693	34.4567	11.05	0.62	B1.5Ia	2	R(4)
116	LSE 63	6736747708089687936	280.0917	-31.9469	12.04	0.42	B1Iabe	1/2	-
117	NGC 6254 1035	4365635279142583424	254.299	-4.0666	11.43	0.84	G0e	1	-
118	OH 15.7 +0.8	4146237904302941440	274.1057	-14.921	16.29	1.06	-	2	R(3)
119	OH 17.7 -2.0	4104128533107792512	277.6288	-14.4793	13.65	1.55	-	2	R(3)
120	OH 345.05 -1.86	5965644393737729664	258.0907	-42.4193	15.61	2.79	-	2	R(3)
121	PG 1704+222	4568163710366782848	256.6924	-22.0978	12.69	0.23	sdB3IHe8	2	-
122	PHL 1580	6831062200578042624	322.6052	-19.3762	12.18	0.1	B2	1/2	R(1)
123	PN G038.7+01.5	4282499452616310912	284.0942	5.8833	12.5	2.91	-	2	R(4)
124	PN PM 1-243	4104509518206051968	278.7396	-13.9802	14.43	1.44	-	2	R(4)
125	RAFGL 6945S	4093773852321518976	272.8321	-21.9166	13.99	1.7	-	2	R(3)
126	SS 441	4210278482327706496	294.073	-3.8903	13.06	-	-	1	-
127	V* AD Aql	4203801018864386944	284.7862	-8.1706	11.28	0.78	kF1hF5cnG5Ib	1	B(7)/V(1)
128	V* AU Vul	1836195688380634368	304.5245	27.7343	9.98	1.57	F3Ie	1/2/3	B(7)/V(1)
129	V* BZ Pyx	5636099047820103424	137.0422	-28.3196	10.91	0.35	F6Ia	1	B(7)/V(1)
130	V* CE Vir	3658327596544582400	207.3213	-1.9291	8.31	0.15	G8III	1	B(1)
131	V* EQ Cas	1993916856117284864	358.222	55.0136	11.3	-	-	1	-
132	V* HP Lyr	2101097215232231808	290.4128	39.9356	10.41	0.33	A3Ia/Iab	1	B(7)/V(1)
133	V* LN Hya	3497154104039422848	194.1256	-26.4603	6.62	0.14	F3Ia	1/2	V(2)
134	V* LX And	332909001084177920	34.9337	40.4562	15.71	0.07	-	1	V(3)
135	V* PS Gem	3159640386918214528	105.9152	10.7703	7.24	0.08	A0	1/2	B(1,2,7)
136	V* RV Col	2902505745786910080	83.9342	-30.8265	8.41	0.15	G5	1/2	V(4)
137	V* RX Cap	6879691160336671744	303.7301	-12.9429	11.37	0.28	G0Iae	1	V(4)
138	V* TT Oph	4386330497453246080	252.3995	3.6317	9.85	0.23	F5pe	1	V(4)
139	V* TX Oph	492705672029913600	256.0004	4.9836	10.05	0.47	F8Iae	1	-
140	V* V1027 Cyg	2030200671149815424	300.6141	30.0737	7.69	2.96	G7Ia	1/2	-
141	V* V1333 Sco	6023926760641310208	246.5849	-34.2869	10.95	1.79	F8	1	B(7)
142	V* V1401 Aql	4190636669164572928	301.2726	-11.5994	6.21	0.33	F2II	1/2	-
143	V* V2053 Oph	4470790101628029440	273.7058	5.2155	9.65	0.63	C	1	B(1,7)
144	V* V340 Ser	4162959693758887424	262.6955	-11.3689	9.3	1.31	F2/3II	2	B(7)
145	V* V360 Cyg	1852749557493420032	317.6479	30.6724	11.08	0.4	F8Ie	1	-
146	V* V399 Cyg	1869102495165230592	312.2852	33.6958	10.96	0.6	G8	1	V(4)
147	V* V400 Sco	4040579578519065728	267.8291	-36.1824	12.7	1.7	-	1	-
148	V* V421 CMa	5617989266685365120	109.0345	-23.4504	10.49	0.95	F5	1/2	B(1,2,7)/V(1)
149	V* V590 Aql	4222177328438155776	304.2856	-4.0519	11.84	0.47	-	1	V(4)
150	V* V652 Her	4449366151908979072	252.0196	13.2618	10.51	0.1	-	1	R(1)
151	V* V709 Car	5258718997589107712	154.8203	-57.3239	9.3	1.41	G8Ia-0	1	B(1,7)/V(4)
152	V* V760 Sgr	4068898810519269248	267.5448	-22.848	10.03	2.04	G5	1	-
153	V* V802 Car	5241806275407841664	165.518	-62.1619	8.62	1.75	F2III	1/2	B(1,2,7)/V(4)
154	V* V811 Ara	5914387846002855296	255.9235	-61.5047	10.68	0.38	-	1	-
155	V* V825 Ara	5921745812182394496	265.0453	-53.7927	11.02	0.49	-	1	-
156	V* V956 Cen	6066902993687172608	198.5344	-54.6929	7.99	0.95	F5Ia/ab	1/2	B(7)/V(4)
157	V* YY Ara	5830750401670303872	250.3352	-59.8752	9.47	0.58	K0:-Me	1	-

**Notes.** Interstellar extinction values ( $A_V^{LS}$ ) are taken from [Stassun \(2019\)](#). Spectral types are taken from Simbad database. **Post-AGB origin:** (1): Simbad database. (2): Torun catalogue. (3): [Suárez et al. \(2006\)](#). **Binary reference (B):** (1): [Kluska et al. \(2019\)](#). (2): Torun catalogue. (3): [Gallardo Cava et al. \(2023\)](#). (4): [Van Winckel et al. \(2014\)](#). (5): [Oomen et al. \(2018\)](#) (6) [Doroshenko et al. \(2016\)](#). (7): [Kluska et al. \(2022\)](#), (8): [Parthasarathy et al. \(2022\)](#). **Variability reference (V):** (1): [Kluska et al. \(2022\)](#). (2): [Kamath et al. \(2022\)](#). (3): [Dubus et al. \(2018\)](#). (4): Simbad database. **Removed reason (R):** (1): very hot star ( $T_{\text{eff}} \geq 24,000$  K). (2): incorrect source identification. (3): without *Gaia* counterpart. (4): already in planetary nebula phase. (5): composite object, blended.

**Table A.2.** Astrometric and evolutionary parameters for the 69 post-AGB stars.

Num	Distance (pc)	Low Dist. (pc)	High Dist. (pc)	$A_V$	$T_{eff}$ (K)	Flag (T)	$Log[L]$	$Log[L]_{min}$	$Log[L]_{max}$	$Mass$ ( $M_{\odot}$ )	$Age_{evo}$ (kyr)	SED	Flag
2	1307	1199	1436	0.50	6500	T3(1)	4.11	4.02	4.20	3.14	< 0.01	disc	-
7	1909	1870	1947	3.85	4250	T3(2)	4.34	4.32	4.37	2.79	1.22	stellar	H
14	6639	5922	7516	1.75	16000	T3(3)	3.75	3.63	3.88	1.33	3.62	stellar	-
15	2271	2160	2400	4.75	3750	T1	3.61	3.56	3.66	1.12	< 0.01	stellar	H
18	3467	3159	3934	0.20	20000	T3(4)	3.55	3.44	3.67	0.93	18.14	shell	H
19	2839	2711	2962	1.60	6500	T3(5)	3.62	3.58	3.66	1.12	5.61	shell	-
21	4734	4150	5414	0.30	21000	T3(6)	3.61	3.47	3.75	0.95	16.54	shell	H
24	9965	9131	11304	0.90	22000	T3(7)	4.30	4.19	4.42	3.81	1.10	stellar	(*)
25	5862	5008	7121	0.73	23000	T3(8)	4.40	4.21	4.58	3.00	9.15	stellar	H
26	4982	4299	6049	1.00	18000	T3(9)	4.24	4.06	4.43	3.63	0.99	stellar	-
27	4718	4214	5732	3.30	6000	T2	4.12	3.95	4.29	3.16	< 0.01	disc	-
29	3858	3644	4143	2.15	20000	T3(6)	4.43	4.37	4.49	4.00	0.69	shell	-
30	3421	3226	3635	3.14	9250	T2	3.87	3.81	3.93	1.98	3.36	shell	-
31	4340	4100	4599	1.97	9000	T2	3.77	3.72	3.83	1.42	3.94	shell	-
33	2822	2677	2982	1.78	20000	T3(6)	4.02	3.97	4.08	2.84	2.14	shell	-
34	5021	4607	5683	1.00	8500	T2	3.76	3.65	3.88	1.38	3.82	shell	-
35	10125	9128	11379	2.25	6750	T2	3.67	3.56	3.78	0.97	9.06	stellar	H
37	10312	8988	12281	< 0.01	11750	T2	3.45	3.28	3.63	< 0.9	13.83	shell	H
39	2916	2712	3196	0.80	7250	T3(10)	3.92	3.84	4.01	2.27	1.49	stellar	(*)
40	2099	1991	2209	2.00	7250	T3(11)	3.94	3.89	3.99	2.40	1.63	shell	H
41	1104	1075	1139	1.00	4250	T3(12)	4.16	4.13	4.19	3.22	< 0.01	disc	-
42	1788	1722	1845	0.82	7250	T3(13)	3.95	3.92	3.98	2.42	1.66	disc	-
43	1567	1503	1632	0.25	8250	T3(14)	3.54	3.50	3.58	0.93	9.14	stellar	H
45	5130	4530	5923	0.70	7000	T3(13)	4.40	4.27	4.53	3.00	9.14	disc	H
47	1708	1647	1782	1.00	8250	T3(11)	3.74	3.71	3.77	1.32	3.57	shell	-
49	3101	2895	3388	0.60	6750	T3(11)	4.51	4.44	4.58	3.00	9.14	stellar	H
51	1921	1830	2016	0.75	6000	T3(11)	3.88	3.83	3.93	2.07	0.28	shell	H
53	1807	1726	1891	0.40	9750	T3(15)	3.38	3.34	3.42	< 1.0	9.67	stellar	-
54	6999	5822	8254	1.40	7000	T3(16)	4.56	4.37	4.74	3.00	9.14	disc	H
58	2310	2165	2481	1.80	8000	T3(11)	3.89	3.83	3.95	2.12	1.34	shell	-
59	1390	1344	1439	0.35	10000	T3(17)	3.57	3.54	3.60	1.07	5.54	stellar	H(*)
60	1410	1356	1465	2.80	5250	T3(11)	3.94	3.90	3.98	2.35	0.58	shell	-
62	5416	5040	5792	2.19	14000	T3(18)	3.51	3.44	3.58	< 1.0	10.68	shell	-
63	3685	3461	3942	1.80	22000	T3(19)	4.15	4.09	4.22	3.32	0.79	shell	-
64	4817	4587	5042	3.00	5500	T3(11)	3.47	3.43	3.51	< 1.0	8.54	shell	-
72	5022	4555	5658	3.35	9000	T3(18)	3.99	3.88	4.09	2.62	1.88	shell	-
75	9082	8261	10230	2.70	7500	T3(11)	3.88	3.78	3.97	2.08	1.29	shell	-
98	6605	5703	7346	2.25	6750	T2	3.38	3.25	3.51	< 1.0	9.14	disc	-
99	2082	2026	2148	3.75	14000	T3(20)	3.91	3.88	3.94	2.23	1.45	shell	-
102	6830	5887	8163	6.75	9750	T3(18)	3.69	3.51	3.87	1.20	8.33	shell	-
111	10863	9455	12375	1.40	15000	T3(21)	4.23	4.09	4.38	2.58	1.83	stellar	H
112	7934	6777	9233	1.75	19000	T3(6)	4.41	4.25	4.57	3.00	1.84	shell	H
113	6437	5646	7505	1.60	16000	T3(22)	3.44	3.29	3.60	< 1.0	11.32	shell	H
114	5354	4801	6044	2.10	19000	T3(23)	4.01	3.89	4.13	2.77	2.07	shell	-
116	7318	6417	8628	1.05	22000	T3(6)	4.12	3.96	4.29	2.26	1.55	shell	H
117	5974	5146	7444	1.00	5750	T3(24)	3.22	3.00	3.43	0.90	7.96	stellar	H
121	7513	6290	9363	0.30	17000	T3(25)	3.34	3.11	3.58	< 0.9	19.81	stellar	H
127	6147	5365	6967	1.20	6250	T3(13)	3.46	3.32	3.61	< 1.0	8.96	disc	-
128	2317	2237	2410	3.50	5750	T3(26)	3.73	3.69	3.78	1.24	8.85	disc	-
129	4556	4246	4929	1.35	6750	T3(27)	3.34	3.26	3.42	< 1.0	9.14	disc	-
132	10720	9413	12080	1.75	8500	T2	4.48	4.35	4.61	3.00	9.15	disc	H
133	1684	1619	1769	1.00	6250	T3(11)	4.02	3.97	4.06	2.71	1.92	disc	-
135	1813	1707	1923	2.40	6000	T3(28)	4.49	4.43	4.55	4.00	4.05	disc	-
136	1850	1806	1893	2.25	5500	T2	3.80	3.78	3.83	1.62	1.53	shell	-
137	7253	6109	8872	0.70	6000	T2	3.40	3.17	3.64	< 0.9	8.29	stellar	H
138	2369	2250	2507	2.25	6500	T2	3.46	3.40	3.53	< 1.0	8.96	stellar	-
139	4682	4285	5128	1.75	6250	T2	3.86	3.77	3.95	1.18	7.64	shell	H
141	3948	3726	4264	2.00	6250	T3(29)	3.37	3.31	3.43	< 1.0	8.96	disc	-
142	727	714	743	1.00	6750	T3(11)	3.47	3.45	3.49	< 1.0	9.14	shell	-
143	4188	3841	4631	1.20	5000	T3(27)	3.67	3.58	3.77	1.18	7.13	disc	-
144	4269	3980	4580	2.00	7250	T2	4.10	4.03	4.16	3.13	0.67	disc	-
145	4795	4442	5245	1.50	6250	T2	3.41	3.32	3.51	< 1.0	8.96	stellar	-
146	4842	4502	5201	2.25	5500	T2	3.58	3.51	3.65	1.08	4.78	stellar	-
147	8617	7584	9718	1.70	4500	T2	3.34	3.21	3.47	< 1.0	6.83	stellar	-
148	5122	4745	5526	10.25	7000	T3(30)	4.13	4.06	4.21	3.22	< 0.01	disc	-
152	2116	1995	2245	2.80	5500	T3(31)	3.40	3.34	3.47	< 1.0	8.54	stellar	-
153	4404	4113	4693	2.00	7500	T3(27)	4.42	4.35	4.48	4.00	9.14	disc	-
156	1535	1468	1606	1.80	6750	T2	3.64	3.60	3.68	1.14	6.95	shell	-
157	2348	2251	2450	2.80	4250	T3(32)	3.41	3.37	3.46	< 1.0	5.58	stellar	-

**Notes.** (\*): Not confirmed previously as post-AGB star in the bibliography. (H): Suspected Halo star.

**References.** Temperatures are: (T1) obtained from SED fitting with  $A_V^{LS}$  from Stassun (2019), (T2) derived from Simbad spectral types, (T3): obtained from the literature (mainly for spectroscopic measurements): (1): Luck (2014), (2): Steinmetz et al. (2020), (3): Jeffery et al. (1998), (4): Napiwotzki et al. (1994), (5): Ting et al. (2019), (6): Mello et al. (2012), (7): Venn et al. (1998), (8): Herrero et al. (2020), (9): Jeffery (1993), (10): Rao et al. (2012), (11): Kamath et al. (2022), (12): de Ruyter et al. (2005), (13): Corporaal et al. (2023), (14): Arentsen et al. (2019), (15): Klochkova et al. (2018), (16): Reyniers & Van Winckel (2001), (17): Kodaira & Philip (1984), (18): Raman et al. (2017), (19): Klochkova (2014), (20): Parthasarathy et al. (2000a), (21): Şahin (2018), (22): Parthasarathy et al. (2000b), (23): Ikonnikova et al. (2020), (24): Wallerstein (1958), (25): Drilling et al. (2013), (26): Kluska et al. (2022), (27): Gielen et al. (2011), (28): Waelkens et al. (1991), (29): Maas et al. (2005), (30): Van Winckel (1997), (31): Buder et al. (2021), (32): Henize (1976).

**Table A.3.** Astrometric and evolutionary parameters for the 29 unconfirmed post-AGB candidates.

Num	Distance (pc)	Low Dist. (pc)	High Dist. (pc)	$A_V$	T(eff) (K)	Flag (T)	Log[L]	Log[L] <sub>min</sub>	Log[L] <sub>max</sub>	SED	Flag
6	4007	3509	4603	0.09	3500	T1	3.19	3.05	3.33	stellar	H
8	7877	7285	8653	< 0.01	7250	T2	2.92	2.83	3.01	stellar	H
16	7633	6920	8251	1.40	11000	T3(1)	3.12	3.03	3.20	stellar	H
23	2569	2382	2815	0.20	11750	T2	2.46	2.38	2.54	stellar	H
32	2138	2058	2229	0.70	9500	T3(2)	3.16	3.12	3.19	stellar	H
44	2568	2429	2706	0.30	7500	T3(3)	2.99	2.94	3.04	stellar	H
46	4893	4514	5338	0.60	6750	T3(4)	3.19	3.11	3.27	stellar	H
48	1446	1391	1510	0.85	22000	T3(5)	2.56	2.52	2.60	stellar	-
57	945	921	964	0.40	6500	T3(6)	2.84	2.82	2.86	disc	-
61	937	926	947	1.00	5750	T3(7)	2.06	2.05	2.07	shell	-
66	1982	1915	2056	0.66	3750	T3(8)	2.37	2.33	2.40	shell	-
69	1952	1895	2002	0.69	3750	T1	2.63	2.60	2.65	shell	-
73	5266	4836	5721	4.00	1000	T3(8)	3.07	2.99	3.15	shell	-
80	3226	3025	3469	5.55	6000	T1	2.76	2.70	2.83	shell	-
81	2504	2408	2629	3.28	6750	T1	2.45	2.41	2.49	shell	-
83	1978	1856	2105	2.50	4000	T3(9)	3.01	2.95	3.06	disc	-
86	4277	3572	5089	5.80	8750	T3(8)	3.00	2.81	3.19	shell	-
87	5204	4054	6718	2.00	3500	T3(8)	1.96	1.64	2.27	shell	-
88	2533	2306	2812	4.53	3750	T1	2.94	2.84	3.04	shell	-
90	4882	4170	5705	3.00	4250	T3(8)	2.27	2.10	2.43	shell	-
91	5991	5520	6694	1.76	8250	T1	3.01	2.91	3.11	shell	-
100	4898	4294	5685	4.79	5750	T1	3.01	2.87	3.16	disc	-
101	6087	5536	6736	0.67	3500	T3(8)	3.15	3.06	3.25	shell	-
105	1694	1631	1768	5.34	4250	T1	2.50	2.46	2.53	disc	-
110	5710	4998	6635	< 0.01	14000	T3(10)	2.79	2.64	2.94	stellar	H
130	1365	1313	1420	0.90	4750	T2	3.21	3.16	3.27	shell	-
149	6299	5704	7065	0.47	4000	T3(9)	3.06	2.95	3.16	stellar	H
154	4714	4378	5080	0.38	4000	T1	3.29	3.22	3.36	stellar	-
155	2123	1943	2310	0.49	3500	T1	2.88	2.80	2.96	stellar	-

**Notes.** (H): Suspected Halo star.

**References.** Temperatures are: (T1) obtained from SED fitting with  $A_V$  from Stassun (2019), (T2): derived from Simbad spectral types, (T3): obtained from the literature (mainly for spectroscopic measurements): (1): Mooney et al. (2004), (2): Venn et al. (1998), (3): Kamath et al. (2022), (4): Gonzalez & Wallerstein (1992), (5): Hunger & Kaufmann (1973), (6): Kluska et al. (2022), (7): Ting et al. (2019), (8): Suárez et al. (2006), (9): Steinmetz et al. (2020), (10): Quin & Lamers (1992).

**Table A.4.** Astrometric and evolutionary parameters for the 14 YSO candidate stars.

Num	Distance (pc)	Low Dist. (pc)	High Dist. (pc)	$A_V$	T(eff) (K)	Flag (T)	Log[L]	Log[L] <sub>min</sub>	Log[L] <sub>max</sub>	SED	Flag
1	1139	1109	1172	1.45	9250	T3(1)	4.28	4.25	4.30	stellar	MC
11	3379	3021	3936	0.79	5000	T3(2)	0.69	0.55	0.82	stellar	-
17	307	305	308	0.07	6250	T2	1.10	1.09	1.10	stellar	-
38	623	619	628	2.75	7500	T3(3)	1.97	1.96	1.98	disc	MC
50	219	217	220	0.50	8750	T2	1.40	1.39	1.40	stellar	-
65	390	387	393	0.93	9500	T2	1.22	1.21	1.22	uncertain	-
84	2915	2503	3473	2.20	5000	T3(3)	0.87	0.70	1.05	shell	-
103	1787	1746	1825	2.25	5500	T3(4)	2.88	2.85	2.90	disc	MC
106	1060	1046	1072	1.32	6750	T3(3)	0.97	0.95	0.98	shell	-
107	482	478	485	0.63	8500	T3(2)	1.38	1.37	1.39	disc	-
108	964	948	981	2.05	6750	T3(3)	0.90	0.89	0.92	disc	MC
109	2186	1944	2596	2.53	6000	T1	0.72	0.56	0.87	shell	-
134	508	497	520	0.07	5500	T1	-0.94	-1.01	-0.87	disc	-
151	4006	3630	4403	6.75	5000	T2	5.32	5.23	5.42	disc	MC

**Notes.** (MC): YSO located in a molecular cloud.

**References.** Temperatures are: (T1) obtained from SED fitting with  $A_V$  from Stassun (2019), (T2): derived from Simbad spectral types, (T3): obtained from the literature (mainly for spectroscopic measurements): (1): Firnstein & Przybilla (2012), (2): Suárez et al. (2006), (3): Raman et al. (2017), (4): Kluska et al. (2022).

**Table A.5.** Astrometric and evolutionary parameters for the 6 stars classified as Supergiant or Horizontal Branch stars.

Num	Distance (pc)	Low Dist. (pc)	High Dist. (pc)	$A_V$	T(eff) (K)	Flag (T)	Log[L]	Log[L] <sub>min</sub>	Log[L] <sub>max</sub>	SED	Flag
4	3506	2918	4516	1.64	7250	T2	1.06	0.79	1.32	stellar	HB/H
5	4503	3936	5076	0.41	9750	T1	1.41	1.28	1.54	stellar	HB/H
20	3661	3424	3917	3.75	16000	T2	4.69	4.62	4.75	disc	S
22	3604	3342	3931	0.06	10750	T1	1.78	1.7	1.86	stellar	HB/H
56	4432	4078	4782	4.00	7500	T3(1)	5.47	5.4	5.55	shell	S
140	3723	3486	3988	3.8	5000	T2	5.13	5.06	5.19	disc	S

**Notes.** (HB): Horizontal Branch star. (S): Supergiant star. (H): Halo star

**References.** Temperatures are: (T1) obtained from SED fitting with  $A_V$  from Stassun (2019), (T2): derived from Simbad spectral types, (T3): obtained from the literature (mainly for spectroscopic measurements): (1): Arentsen et al. (2019).